Environmental Science & Technology

Article

pubs.acs.org/est

Novel Method for Nitrogen Isotopic Analysis of Soil-Emitted Nitric Oxide

Zhongjie Yu* and Emily M. Elliott

Department of Geology and Environmental Science, University of Pittsburgh, Pittsburgh, Pennsylvania 15260, United States

Supporting Information

ABSTRACT: The global inventory of NO_x (NO_x = NO + NO_2) emissions is poorly constrained, with a large portion of the uncertainty attributed to soil NO emissions that result from soil abiotic and microbial processes. While natural abundance stable N isotopes ($\delta^{15}N$) in various soil N-containing compounds have proven to be a robust tracer of soil N cycling, soil $\delta^{15}N$-NO is rarely quantified due to the measurement difficulties. Here, we present a new method that collects soil-emitted NO through NO conversion to NO_2 in excess ozone (O_3) and subsequent NO_2 collection in a 20% triethanolamine (TEA) solution as nitrite and nitrate for $\delta^{15}N$ analysis using the denitrifier method. The precision and accuracy of the method were quantified through repeated collection of an analytical NO tank and intercalibration with a modified EPA NO_x collection method. The results show that the efficiency of NO conversion to NO_2 and subsequent NO_2 collection in the TEA solution is >98% under a variety of controlled conditions. The method precision (1σ) and accuracy across the entire analytical procedure are ±1.1‰. We report the first analyses of soil $\delta^{15}N$-NO (−59.8‰ to −23.4‰) from wetting-induced NO pulses at both laboratory and field scales that have important implications for understanding soil NO dynamics.

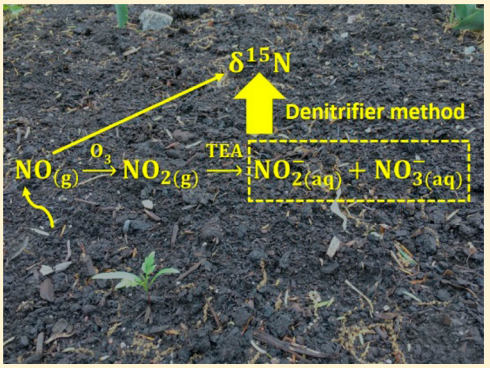

INTRODUCTION

Emissions of nitrogen oxides (NO_x = NO + NO_2) degrade air quality and affect the global tropospheric chemistry,[1,2] posing a significant danger to ecosystem and human health.[3−6] Although fossil fuel combustion is currently the largest source of atmospheric NO_x,[7,8] NO is also produced in and emitted from natural and fertilized soils.[9−11] Due to the spatial segregation of different NO_x sources and the short boundary layer lifetime of NO_x, there are substantial areas of the world (e.g., tropical and agricultural regions) where the local NO_x budget is controlled exclusively by soil NO emissions.[3,7,12−15] In these regions, soil NO emissions govern the formation and lifetime of tropospheric ozone (O_3) and hydroxyl radical, driving reaction chains that produce environmentally important trace gases (e.g., nitric acid and peroxyacetyl nitrate) and biogenic secondary aerosols.[4,13,16]

Various processes, both microbial[10,17−19] and abiotic,[20−22] are capable of producing NO in soils. Although the strong dependence of soil NO emission on edaphic and climatic factors has long been demonstrated by laboratory and field studies,[23−27] a process-based understanding of soil NO dynamics is lacking.[14,28] More importantly, soil NO emission often exhibits an episodic nature (e.g., time scale of minutes), with pulselike emission events often being triggered by rewetting of dry soils.[12,13,29−33] In dry agricultural soils, massive NO pulses triggered by coupled fertilization and precipitation during warm seasons can result in daily O_3 enhancement up to 16 ppbv.[13] Unfortunately, the sources of and processes controlling the pulsed soil NO emission are still mysterious,[13,14] making it difficult to model and up-scale field-observed NO fluxes. While empirical bottom-up models estimate that soil NO emission accounts for about 15% of the global NO_x inventory,[1] inversion of satellite-based NO_2 observations indicate significant underestimation of soil NO emission (e.g., up to a factor of 3) at various spatiotemporal scales.[7,12−16,29,34] Indeed, with the substantial reductions in NO_x emissions from combustion sources in many countries,[2,35] soils as a source of atmospheric NO_x may be more important than we thought, and there is a pressing need to elucidate mechanisms underlying soil NO dynamics.[13,14]

Stable N isotope compositions at natural abundances (notated as $\delta^{15}N$) in various soil N-containing compounds are a robust tracer of soil N cycling.[36−39] Incorporation of $\delta^{15}N$-NO measurements into the soil N isotope systematics is expected to provide new process-level information on key mechanisms regulating NO production and consumption in soil. Moreover, there is a growing interest in using $\delta^{15}N$ of atmospheric nitrogen oxides (e.g., NO_2 and nitrate (NO_3^-)) as a tracer to partition NO_x emission sources over large spatial and temporal scales.[40−43] This interest stems from the observations that NO_x emitted from different sources has distinct $\delta^{15}N$

Received: January 31, 2017
Revised: May 2, 2017
Accepted: May 3, 2017
Published: May 3, 2017

DOI: 10.1021/acs.est.7b00592
Environ. Sci. Technol. 2017, 51, 6268−6278

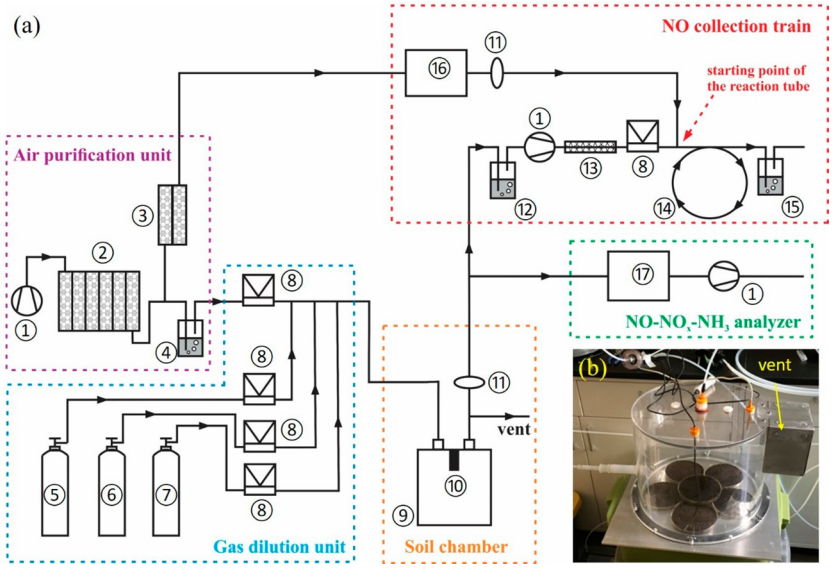

Figure 1. (a) Schematic of the DFC system (not to scale) consisting of the following: (1) diaphragm pump, (2) air purification columns, (3) drying columns, (4) humidifier, (5–7) NO, NO_2, and NH_3 reference tanks, (8) mass flow controller, (9) flux chamber, (10) temperature and relative humidity sensor, (11) in-line PTFE particulate filter assembly, (12) HONO scrubber, (13) moisture exchanger, (14) reaction tube, (15) gas washing bottle containing TEA solution, (16) O_3 generator, (17) NO–NO_x–NH_3 analyzer. (b) Picture showing the field chamber. Specifications of each component of the DFC system are given in Table S2 in the Supporting Information.

values[44−49] and that soil-emitted NO has lower δ^{15}N values than NO_x from other natural and anthropogenic sources.[50−52]

Despite its promising potential, soil δ^{15}N-NO is rarely measured due to the intermittent nature and low magnitudes of soil NO emission. A summary of published NO_x collection methods is provided in Table S1 in the Supporting Information, highlighting that none of the existing methods have been rigorously verified for their suitability for soil-emitted NO. In pioneering work, Li and Wang[50] fertilized a soil monolith in the laboratory and collected NO by first converting NO to NO_2 using a chromium trioxide (CrO_3)-impregnated solid oxidizer and then trapping the converted NO_2 in an annular denuder as nitrite (NO_2^-) for δ^{15}N analysis. However, it is well documented that the NO oxidation efficiency of the CrO_3 oxidizer varies dramatically with the sample relative humidity (RH) (e.g., <50% at RH > 60%).[53,54] Due to this overlooked humidity interference, it is unclear whether N isotopic fractionation can occur during the NO oxidation under varying soil conditions. Recently, Fibiger et al.[55] and Wojtal et al.[56] presented a NO_x collection method that utilizes a $KMnO_4$ + NaOH solution to actively collect NO_x as NO_3^- for δ^{15}N-NO_x determination. The sample δ^{15}N-NO_x must be calculated using an isotope mass balance due to a high reagent blank in the solution (5–7 μM NO_3^-, δ^{15}N = ~2‰).[49,55] While the precision of this approach is ±1.5‰, the method is incompatible for δ^{15}N-NO measurement of low and diffuse soil NO emissions. This is because larger error is propagated from the isotope mass balance calculation if the concentration and δ^{15}N value of collected soil NO are significantly lower than those of the blank.

Here, we present a new method for soil δ^{15}N-NO determination (hereafter, the DFC-TEA method). This method collects NO through NO conversion to NO_2 in excess O_3 and subsequent NO_2 collection in a triethanolamine (TEA) solution as NO_2^- and NO_3^- for δ^{15}N analysis. The NO collection approach is coupled to a soil dynamic flux chamber (DFC) system for simultaneous NO flux and δ^{15}N-NO measurements. Both laboratory and field method verifications have been conducted to demonstrate the suitability of the DFC-TEA method for accurate and precise soil δ^{15}N-NO determination.

EXPERIMENTAL SECTION

DFC System Setup. The DFC is a system that has been developed to continuously measure soil–atmosphere fluxes of various compounds including NO.[18,19] A schematic of the developed DFC system is shown in Figure 1. The system consists of five components: the air purification unit, gas dilution unit, flux chamber, NO–NO_x–NH_3 analyzer, and NO collection train. Zero air free of NO_x and O_3 is produced in the air purification unit for purging the flux chamber and providing air to an O_3 generator (model 146i, Thermo Fisher Scientific) in the NO collection train. NO, NO_2, and ammonia (NH_3) concentrations in the chamber headspace are measured alternately by a chemiluminescent analyzer (model 17i, Thermo Fisher Scientific) at 10 s intervals for flux calculations. For method development, reference NO, NO_2, and NH_3 from three analytical tanks were diluted into the purging flow to simulate soil gas emissions inside the chamber. Two versions of the DFC system were developed for laboratory and field experiments. In the laboratory DFC system, a 1 L Teflon flow-through jar is used as the flux chamber. For the field DFC system, we fabricated a cylindrical flow-through chamber (39 cm i.d. and 30 L inner volume; Figure 1b), following considerations[57,58] for minimizing pressure differentials in the chamber headspace. Control tests indicate that NO transmission from the chamber is greater than 98.3%. Details about the flux measurement, the chamber tests, and the specifications for each DFC component are provided in the Supporting Information.

NO Collection Train. To collect NO for δ^{15}N-NO analysis, a Teflon-coated diaphragm pump is used to sample the chamber air passing through the NO collection train (Figure 1). The sample flow rate (1.6 standard liter per minute (slpm)) is controlled by a mass flow controller. For the NO conversion in

DOI: 10.1021/acs.est.7b00592
Environ. Sci. Technol. 2017, 51, 6268–6278

excess O_3, a length of Teflon tubing (9.5 mm i.d., ca. 240 cm length) serves as the reaction tube. An O_3 flow of 0.4 slpm, produced from photolysis of O_2 in zero air at 185 nm by the O_3 generator, is mixed with the sample flow at the starting point of the reaction tube (Figure 1). To prevent generation of HO_x radicals during the photolysis, water vapor is removed from the zero air using two drying columns and a Teflon filter is attached before the O_3 addition point to decompose remaining HO_x radicals.[59] The long-term (5 months) average O_3 concentration after the mixing of the sample and O_3 flows was 2911 ± 32 ppbv as measured by an O_3 monitor (model 202, 2B Technologies). The flow leaving the reaction tube is forced to pass through a 500 mL gas washing bottle with a fritted cylinder containing a solution of TEA (Fisher Scientific, certified grade) in water (20% (v/v), 70 mL). The stopper of the gas washing bottle was lengthened so that 70 mL of the solution just covered the frit.

Determination of the Reaction Time. Reaction of NO with excess O_3 forms NO_2 (R1 in Table S3 in the Supporting Information). In a dark environment, the efficiency of NO to NO_2 conversion is limited by the formation of higher nitrogen oxide species (i.e., nitrate radical (NO_3) and dinitrogen pentoxide (N_2O_5); R2−R5 in Table S3 in the Supporting Information).[59−63] To model the NO conversion in the reaction tube, the reaction time is needed. Following the method of Fuchs et al.,[61] the reaction time in the reaction tube was experimentally determined by sampling zero air that contained a constant NO concentration (27 ppbv) using the NO collection train and varying the excess O_3 concentrations (266−2890 ppbv). The ending point of the reaction tube was attached to the sampling inlet of the chemiluminescent analyzer for NO concentration determination. The NO concentration decay was then fitted to a single-exponential function assuming pseudo-first-order loss of NO in excess O_3 (details are described in the Supporting Information). Due to the inner tubing of the chemiluminescent analyzer, the estimated reaction time essentially includes the reaction tube plus the analyzer inner tubing. To correct this overestimate, the reaction time of the inner tubing was estimated by repeating the experiment with the mixing point of the sample and O_3 flow directly attached to the analyzer inlet for NO concentration determination.

Preparation of the TEA Solution. Triethanolamine is a tertiary amine and has long been used to scrub acidic gases in fuel gas treating processes and to coat passive filters for ambient NO_2 monitoring.[52,64−66] We used a 20% TEA solution for NO_2 collection. Its reagent N blank was determined to be 0.12 ± 0.04 μM (details are given in the Supporting Information).

It is reported that aging of the TEA solution can cause a significant efficiency decrease in collecting NO_2.[55] This aging problem may occur to a greater degree with more diluted TEA solutions.[55] Therefore, to minimize alteration of TEA from its original state, we subsampled new TEA (i.e., from a freshly opened bottle) into 15 mL glass vials in a glovebox with a 95% N_2 + 5% H_2 atmosphere to avoid contact with ambient air. The vials were then capped, tightly wrapped with Parafilm, sealed in Ziploc bags, and stored in the dark at 4 °C until further use. One glass vial was opened to make a fresh 20% TEA solution immediately prior to each sample collection. The storage time of TEA used in this study was up to approximately 4 months since subsampling.

Measurement of NO_2^- and NO_3^- in the TEA Solution. Both NO_2^- and NO_3^- can be produced from the reaction between NO_2 and TEA.[64−66] The NO_2^- + NO_3^- concentration in the TEA collection samples was measured using a modified spongy cadmium method.[67] The detailed measurement protocol is given in the Supporting Information. Control tests using 10 μM NO_2^- or NO_3^- in 20% TEA solution indicate that the precision (1σ, n = 8) of the method is ±0.09 and ±0.36 μM for NO_2^- and NO_3^- measurements, respectively. Due to the multiple reduction and neutralization steps during the measurements and the N blank inherent to the 20% TEA solution (~0.12 μM), standards were always prepared in 20% TEA solution for concentration calibration.

Isotopic Analysis. The isotopic composition of collected NO_2^- and NO_3^- in the TEA solution was measured using the bacterial denitrifier method.[68,69] In brief, denitrifying bacteria lacking the N_2O reductase enzyme (*Pseudomonas aureofaciens*) are used to convert 5−20 nmol of NO_2^- and NO_3^- into gaseous N_2O. Using He as a carrier gas, the N_2O is then purified in a series of chemical traps, cryofocused, and finally analyzed on a GV Instruments Isoprime continuous flow isotope ratio mass spectrometer at m/z 44, 45, and 46 at the University of Pittsburgh *Regional Stable Isotope Lab for Earth and Environmental Science Research*.

Special considerations were taken during the isotopic analysis to ensure precise and accurate measurement of the $\delta^{15}N$ in the TEA collection samples. First, the TEA collection samples were neutralized using 12 N HCl to pH ≈ 8 before sample injection to avoid overwhelming the buffering capacity of the bacterial medium.[70] Second, in light of the expected low $\delta^{15}N$ of soil-emitted NO[50−52] and the presence of NO_2^- as the dominant collection product (see below), a NO_2^- isotopic standard with a low $\delta^{15}N$ value (KNO_2, RSIL20, USGS Reston; $\delta^{15}N$ = −79.6‰, $\delta^{18}O$ = 4.5‰)[70] was used together with other international NO_3^- reference standards (IAEA-N3, USGS34, and USGS35) to calibrate the $\delta^{15}N$ and $\delta^{18}O$ measurements. Third, following the IT principle (i.e., identical treatment of the sample and reference material), a blank-matching strategy was used to make the isotopic standards in the same matrix (i.e., 20% TEA) as the collection samples and to match both the molar N amount and injection volume (±5%) between the collection samples and the standards (Figure 2). This ensures

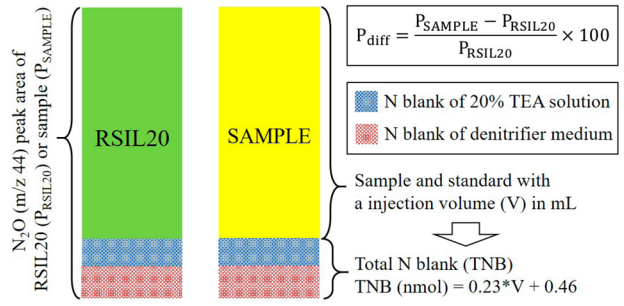

Figure 2. Illustration of the blank-matching strategy for correcting N blanks associated with the TEA solution and denitrifier method.

that the isotopic interference of any blank N associated with the bacterial medium[68,71] and the TEA solution is minimized. The percentage difference (P_{diff}) in the major N_2O (m/z 44) peak area between each collection sample and RSIL20 measured within the same batch was calculated to quantify how precisely the blank-matching strategy was implemented (Figure 2). Finally, the $\Delta^{17}O$ ($\Delta^{17}O = \delta^{17}O - 0.52(\delta^{18}O)$)[72] of the analyte N_2O was independently measured for collected samples with

DOI: 10.1021/acs.est.7b00592
Environ. Sci. Technol. 2017, 51, 6268−6278

sufficient concentration for 50 nmol injection using the N_2O thermal decomposition method.[73] The resolved $\Delta^{17}O$ was then used to correct the isobaric interference from the NO oxidation by O_3 on the $\delta^{15}N$ analysis according to Kaiser et al.[73]

Quantification of the Method Precision and Accuracy. The precision of the DFC-TEA method was quantified through repeated NO collection using the reference NO tank (50.4 ppmv). The collection was conducted under a variety of conditions, including differing NO concentrations (12−749 ppbv), chamber temperatures (11.5−30.8 °C), RH (27.1−92.0%), and purging flow rates in the field chamber (5−20 slpm) and the coexistence of NH_3 in high concentrations (500 ppbv). In light of the high temporal variability of soil NO emission, we limited the collection time for each sample to be less than 2 h. Given that soils can produce and emit nitrous acid (HONO)[74,75] and that HONO positively interferes with NO_2 collection in TEA solution,[65] interference of the $\delta^{15}N$-NO analysis by soil HONO emission was minimized by forcing the sample flow to pass through a HONO scrubber (250 mL fritted gas washing bottle containing 50 mL of 1 mM phosphate buffer solution at pH 7.0)[76] before entering the NO collection train.

While there is no certified isotopic standard for gaseous NO, the accuracy of the DFC-TEA method was evaluated through intercalibration with a modified EPA NO_x collection method. A detailed description of the modified EPA method has been provided by Felix et al.[44] and Walters et al.[47] In brief, gas samples from the reference NO and NO_2 tanks were collected directly into evacuated a 1 L borosilicate gas sampling bulb containing 10 mL of a NO_2-absorbing solution (H_2SO_4 + H_2O_2) on a vacuum line. The absorbing solution oxidizes NO_2 into NO_3^-. For the NO collection, the collection was terminated with a small vacuum remaining in the bottle. The bottle was then quickly vented to the laboratory atmosphere to allow introduction of O_2 into the bottle for the conversion of NO to NO_2.[77] After the collection, the bottles were allowed to stand for 1 week with occasional shaking to facilitate the conversion of NO_x to NO_3^-. The residual NO_x headspace concentration was measured after a 1 week period and indicated that the collection was 100%. The absorbing solution was then collected and neutralized for $\delta^{15}N$ analysis using the denitrifier method. The results show that the NO and NO_2 tanks had $\delta^{15}N$ values of −71.4‰ ± 0.5‰ (n = 4) and −39.8‰ ± 0.2‰ (n = 3), respectively.

Laboratory Soil δ^{15}N-NO Measurements. To test the DFC-TEA method using real soil samples, approximately 4 kg of soil was collected from the upper 10 cm of an urban forest soil in Pittsburgh, PA. Before use, the soil samples were sieved by passing through a 2 mm sieve and air-dried for 14 days. To trigger NO pulses, 35 g of the air-dried soil samples was added to the Teflon jar, mixed thoroughly, and wetted by deionized water to achieve 100% water holding capacity. With the continuous purging of the jar headspace, the soil samples were subject to drying over the next 48 h, and NO was collected periodically for $\delta^{15}N$-NO analysis.

Field Soil δ^{15}N-NO Measurements. To verify the DFC-TEA method under varying field conditions, the field DFC system was deployed using the University of Pittsburgh *Mobile Air Quality Laboratory* to measure $\delta^{15}N$-NO in a field soil rewetting experiment (see Figure S10 in the Supporting Information for the field setup). A waterproof tarp (300 cm × 240 cm) was erected over a fallow, urban plot in Pittsburgh, PA, for 2 weeks (Aug 15−29, 2016) to exclude precipitation inputs. After the drying period, four soil plots were respectively wetted on four consecutive days using 500 mL of Milli-Q water, 20 mM KNO_3 ($\delta^{15}N$ = 46.5‰ ± 0.3‰), 10 mM $NaNO_2$ ($\delta^{15}N$ = 1.0‰ ± 0.4‰), and 20 mM NH_4Cl ($\delta^{15}N$ = 1.7‰ ± 0.1‰) solutions. These N amendment solutions were chosen because they are common drivers of major NO-producing processes.[31,36] Previous studies have reported that common $\delta^{15}N$ values of N fertilizers are not very different from 0‰ (e.g., −4.4‰ to +0.3‰),[78] while $\delta^{15}N$ values of atmospherically deposited NO_2, NO_3^-, and NH_4^+ could vary over a wider range (e.g., −10‰ to +15‰), depending on source contributions.[42,79] Hence, the $\delta^{15}N$ values of the amended NO_2^- and NH_4^+ are within the environmentally relevant range, whereas the $\delta^{15}N$ of the added NO_3^- is significantly higher. The NO, NO_2, and NH_3 fluxes were continuously measured before and after the soil rewetting, and NO was collected periodically for the $\delta^{15}N$-NO analysis.

RESULTS AND DISCUSSION

We evaluate each step in the NO collection and report isotopic results that document the overall precision and accuracy of the $\delta^{15}N$-NO analysis. We then present $\delta^{15}N$-NO measurements from laboratory and field soil rewetting experiments that demonstrate the utility of the DFC-TEA method for resolving soil NO dynamics.

NO Conversion in Excess O_3. The reaction time of the inner tubing of the chemiluminescent analyzer and the reaction tube plus the inner tubing were estimated to be 1.4 and 6.4 s, respectively, resulting in a reaction time of the reaction tube of 5 s at the measured flow temperature (22 °C) (Figure S7 in the Supporting Information). This estimated reaction time is consistent with the residence time calculated from the assumption of plug flow in the reaction tube. On the basis of this reaction time and the average O_3 concentration of 2911 ppbv, numerical model calculations including reactions R1−R5[80] and NO_3 loss on the interior tubing wall (R6 in Table S2 in the Supporting Information)[81] indicate that NO is quantitatively converted in the reaction tube and that the specific conversion of NO to NO_2 is between 98.7% and 99.0% over a wide range of NO concentrations (0−1000 ppbv) at 22 °C (Figure S8a in the Supporting InformationI). Notably, the remaining NO from the conversion exists primarily as N_2O_5 (Figure S8b in the Supporting Information).

Deviations from the controlled laboratory condition in the field may result in variations in the modeled NO conversion efficiency.[61] We therefore modeled the effects of temperature variation and soil emission of biogenic volatile organic carbon (BVOC)[82] on the NO conversion (reactions R7 and R8 in Table S2 in the Supporting Information).[83] The results indicate that the conversion of NO to NO_2 is not likely to fall below 98% over a temperature range of 0−40 °C in conjunction with high BVOC emissions (e.g., 100 ppbv isoprene in the chamber) (details on the extended modeling are given in the Supporting Information). In addition, slight variations in the reaction time may result from changes in the temperature and pressure of the sample flow (e.g., a pressure increase induced by the attachment of the gas washing bottle). While the effect of these variations on the NO conversion is difficult to empirically quantify, any uncertainty in converting NO under the tested conditions is reflected in the overall method precision and accuracy for the $\delta^{15}N$-NO measurement.

NO_2 Collection in the TEA Solution. The 20% TEA solution was 100% efficient at collecting NO_2. This was confirmed by collecting a flow of reference NO_2 at 1 ppmv

DOI: 10.1021/acs.est.7b00592
Environ. Sci. Technol. 2017, 51, 6268−6278

Table 1. Summary of the Reference NO and NO_2 Tank Collection Using the DFC-TEA Method under Varying Environmental Conditions[a]

sample	time (min)	T (°C)	RH (%)	NO_2^- + NO_3^- conc (μM)	recovery[b] (%)	NO_2^- fraction (%)	P_{diff} (%)	$\delta^{15}N$[c] (‰)	$\Delta^{17}O$ (‰)
NO_2 Collection—Laboratory DFC System									
1002 ppbv NO_2 (n = 4)	135	23.7	25.3	132.5	101.4	87.4	3.3	−40.1	
standard error (1σ)				4.7	3.6	0.3	5.1	0.8	
NO Collection—Laboratory DFC System									
12 ppbv NO (n = 3)	120	23.0	44.6	1.4	95.0	97.0	−0.7	−73.0 (−71.7)	
34 ppbv NO (n = 4)	120	24.8	27.1	4.1	100.7	93.1	−1.2	−70.3 (−69.2)	
101 ppbv NO (n = 4)	120	23.1	34.2	11.9	98.2	94.0	0.7	−71.0 (−69.9)	18.8
749 ppbv NO (n = 4)	120	22.8	47.5	14.2	99.3	90.7	3.5	−70.6 (−69.4)	20.6
NO Collection—Laboratory DFC System—Temperature Effect									
34 ppbv NO (n = 4)	120	11.5	92.0	4.0	99.8	89.3	2.4	−71.1 (−70.0)	
101 ppbv NO (n = 4)	120	30.8	28.8	11.8	98.7	89.5	3.6	−70.8 (−69.7)	20.0
NO Collection—Laboratory DFC System—Interference									
34 ppbv NO + 500 ppbv NH_3 (n = 3)	120	23.0	33.1	4.0	99.5	88.2	−3.8	−70.1 (−69.0)	
101 ppbv NO + 500 ppbv NH_3 (n = 4)	120	23.1	46.5	11.7	97.5	91.5	2.6	−71.2 (−70.2)	19.5
101 ppbv NO + HONO (n = 4)	120	22.3	89.7[d]	11.6	96.7	89.8	2.8	−71.0 (−69.9)	19.6
NO Collection—Field DFC System[e]									
25 ppbv NO (n = 4)	120	21.4	40.8	3.1	103.9	94.3	4.3	−72.9 (−71.7)	
34 ppbv NO (n = 4)	120	21.9	50.4	3.9	97.6	92.8	−1.8	−70.7 (−69.6)	
56 ppbv NO (n = 3)	120	21.2	44.8	6.2	96.0	92.9	−2.0	−71.5 (−70.4)	
101 ppbv NO (n = 4)	120	21.7	36.6	11.7	97.1	89.5	1.0	−71.0 (−69.9)	19.5
mean					**98.5**	**91.7**	**1.1**	**−71.1 (−70.0)**	**19.7**
standard error (1σ)					**3.5**	**3.4**	**5.1**	**1.1 (1.1)**	**0.8**

[a]The complete data set is given in Table S4 in the Supporting Information. Out of 56 NO and NO_2 tank collection samples, 52 samples yielded consistent results and 4 samples were detected as outliers on the basis of erroneous concentrations. These outliers might result from contamination or insufficient flushing of the tubing connecting the NO tank and thus were not included in this table. [b]NO (NO_2) recovery was calculated by dividing the measured NO_2^- + NO_3^- concentration by the theoretical concentration calculated using the collection time, sample flow rate (1.6 slpm), NO (NO_2) concentration, and TEA solution volume. The TEA solution volume was corrected for evaporative loss by weighing the gas washing bottle containing the solution before and after each sample collection. [c]Relative to N_2 in the air. $\delta^{15}N$ values before the isobaric correction are shown in parentheses. [d]RH was measured after the HONO scrubber instead of in the Teflon chamber. [e]The chamber purging flow rates were 20, 15, 9, and 5 slpm for the 25, 34, 56, and 101 ppbv NO collection, respectively.

using the laboratory DFC system (Table 1). Importantly, because the 20% TEA solution foams rigorously upon sparging, the applied total flow rate (1.6 slpm sample flow plus 0.4 slpm O_3 flow) was chosen to avoid solution spill. We have also tested a TEA solution from another brand (BioUltra) that foams much less rigorously (coarse bubbles). However, a consistently low collection efficiency (<90%) was found using this TEA solution. Thus, it is important to test the TEA solution using a NO_2 tank to ensure 100% NO_2 collection efficiency.

The measured NO recovery of the NO tank collection samples ranged between 95.0% and 103.9% across the individual sets of collection conditions, with an average value of 98.5% ± 3.5% (Table 1). A nonparametric Kruskal–Wallis test indicates that none of the controlled factors (e.g., NO concentration, temperature, purging flow rate, and choice of the laboratory or field DFC systems) had a significant effect on the NO recovery (P > 0.05). The deviations from 100% NO recovery likely reflect inefficiencies in the NO conversion (see above), the high uncertainty in the NO_3^- concentration determination (e.g., for the 12 and 25 ppbv NO collection samples), and/or NO loss within the system (e.g., NO loss in the HONO scrubbing solution and on the interior wall of the field chamber). Importantly, the high and consistent NO recovery is direct evidence that the subsampling was effective at minimizing the TEA aging problem, if any, for a storage time of at least 4 months.

For all the tank collection samples (n = 52), about 90% of the collected NO or NO_2 was in the form of NO_2^-, and the remainder was NO_3^- (Table 1). A 90% NO_2^- + 10% NO_3^- stoichiometry has been previously reported for active NO_2 sampling using TEA-coated cartridges.[65] While a satisfactory explanation for the NO_3^- production cannot be given at this time,[65] the observed stoichiometry is best approximated by the redox reaction between NO_2 and TEA in the presence of water that gives a theoretical 1:1 conversion of NO_2 to NO_2^-.[64,65,84] It is well-known that N_2O_5 hydrolyzes in water as HNO_3[85] and is preserved as NO_3^- in alkaline solutions. However, whether N_2O_5 produced in the NO conversion can be collected in the TEA solution as NO_3^- is not possible to quantify in this case due to the high uncertainty in the NO_3^- concentration determination (i.e., ±0.36 μM) but will be the subject of future research.

It is worth noting that the collection efficiency of the 20% TEA solution could decrease over longer collection periods due to the presence of O_2, O_3, and CO_2 in the sample flow that can compete with NO_2 for TEA oxidation and decrease the solution pH. Given that the DFC-TEA method described here is developed to characterize transient variations of soil NO emissions, use of 20% TEA solution for prolonged collection

DOI: 10.1021/acs.est.7b00592
Environ. Sci. Technol. 2017, 51, 6268–6278

(i.e., >2 h) should be further investigated to ensure high and consistent collection efficiency.

Analytical Uncertainty of the Denitrifier Method and the Total N Blank. The pooled standard deviation for each of the isotopic standards made in 20% TEA solution and measured along with individual sample sets was 0.3‰, 0.3‰, and 0.8‰ for $\delta^{15}N$ of IAEA-N3, USGS34, and RSIL20, respectively, 0.7‰ and 0.7‰ for $\delta^{18}O$ of IAEA-N3 and USGS34, respectively, and 1.2‰ for $\Delta^{17}O$ of USGS35. The lower precision of the $\delta^{15}N$ analysis of RSIL20 (0.8‰ relative to 0.3‰ for other standards) is due to the larger uncertainty in measuring diluted RSIL20 solutions that require large injection volumes (Figure 3a). To further understand this volume

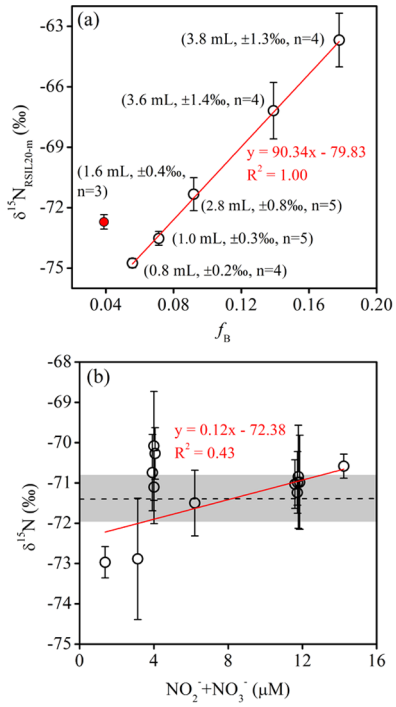

Figure 3. (a) Measured $\delta^{15}N$ of RSIL20 ($\delta^{15}N_{RSIL20\text{-}m}$) as a function of the fraction of analyte N_2O-N derived from the total N blank (f_B). The sample injection volume, standard deviation of $\delta^{15}N_{RSIL20\text{-}m}$, and number of replicates for the individual runs are given in parentheses. The red dot (56 ppbv collection sample) was not included in the linear regression. (b) Measured $\delta^{15}N$ of the NO collection sample as a function of the sample NO_2^- + NO_3^- concentration. The dashed line and the shaded area represent the mean ± 1σ of the $\delta^{15}N$ of the NO tank measured using the modified EPA NO_x collection method.

dependence, we estimated the total N blank associated with the $\delta^{15}N$ analysis of the TEA samples (i.e., TEA N blank + blank N associated with the denitrifier medium[68,71]) by quantifying shrinkage of the N isotope ratio scale between USGS34 and RSIL20 measured in each run of the TEA collection samples[86] (more details are given in the Supporting Information). The results show that the fractional blank size (f_B) ranged between 0.04 and 0.18 across different runs and was significantly, positively correlated with the sample volume and the measured $\delta^{15}N$ of RSIL20 ($\delta^{15}N_{RSIL20\text{-}m}$) (Figure 3a). Fitting a linear equation to the molar amount of the total N blank and the sample volume indicates that the N blank likely consisted of a constant component of 0.46 ± 0.12 nmol and a sample volume-dependent component of 0.23 ± 0.06 nmol·mL^{-1} (Figure S5 in the Supporting Information; Figure 2); this is consistent with the blank size estimated by injecting blank 20% TEA solution (details are provided in the Supporting Information). From the linear relationship between f_B and $\delta^{15}N_{RSIL20\text{-}m}$, the $\delta^{15}N$ of the blank N appears to be ~10‰ across different runs (Figure 3a). These consistent and predictable behaviors of the total N blank indicate with a high degree of confidence that its isotope effect is implicitly corrected during the $\delta^{15}N$ analysis using the blank-matching strategy.

Isobaric Interference from Mass-Independent Oxygen Isotopic Composition. The $\delta^{18}O$ of RSIL20 calibrated against IAEA-N3 and USGS34 ranged from −25.8‰ ± 0.9‰ to −22.7‰ ± 1.5‰ across different runs, with an average of −23.7‰ ± 1.1‰. This results in an isotopic offset of about 28‰ between the measured apparent $\delta^{18}O$ and the "true" $\delta^{18}O$ (4.5‰) of RSIL20, in line with the branching fractionation between NO_3^- and NO_2^- during denitrification (25−30‰).[70] This implies that the oxygen isotopic exchange between NO_2^- and water is limited in the alkaline TEA solution. Not surprisingly, positive $\Delta^{17}O$ values were observed in the N_2O generated from collected samples. To understand the transfer of the $\Delta^{17}O$ anomaly from O_3 during the NO conversion, a theoretical $\Delta^{17}O$ of the NO_2 produced from the NO + O_3 reaction (R1 in Table S2 in the Supporting Information) was calculated to be 22.5‰ ± 1.8‰ (details are provided in the Supporting Information). This theoretical $\Delta^{17}O$ value is not very different from measured $\Delta^{17}O$ values, which had an average of 19.7‰ ± 0.8‰ across different runs (Table 1), indicating that the NO + O_3 reaction essentially dominated during the NO conversion. The measured $\Delta^{17}O$ values led to a 1.0−1.2‰ correction of the measured $\delta^{15}N$ values. For samples without sufficient concentrations for $\Delta^{17}O$ measurement, the average $\Delta^{17}O$ value (19.7‰) was used for the correction. This is not a complete correction, in that the expression of the isobaric interference depends on f_B relative to each sample. Nevertheless, the resultant overcorrection for the $\delta^{15}N$ of the low-concentration samples is <0.2‰ in this case, and is not explicitly addressed.

Overall Accuracy and Precision of the DFC-TEA Method. The $\delta^{15}N$ of the NO tank collection samples after the isobaric correction ranged from −73.0‰ to −70.1‰ across the individual sets of the collection conditions (Table 1), with an average value of −71.1‰ ± 1.1‰. P_{diff} ranged between −9.8% and +15.9% and was 1.1% ± 5.1% on average (Table 1). P_{diff} was not sensitive to the sample concentration used for blank-matching, indicating that the sample concentrations were precisely measured and diluted for the $\delta^{15}N$ analysis (Figure S6a in the Supporting Information). A nonparametric Kruskal−Wallis test indicates that none of the controlled factors or P_{diff} had a significant effect on the $\delta^{15}N$ values ($P > 0.05$; Figure S6b in the Supporting Information). The DFC-TEA method and the EPA NO_x collection method generally agree within 0.3‰, although discrepancies within individual sets of collected samples ranged from −1.3‰ to +1.6‰. The largest discrepancies between the two methods occurred with the lowest sample concentrations (i.e., 12 ppbv NO collection samples) (Figure 3b). For these low-concentration samples, isotopic analyses were conducted on 5 nmol of NO_2^- + NO_3^- (achieved with a 3.8 mL injection of the collection samples) and of an f_B of 0.18. Therefore, although P_{diff} did not correlate with the sample concentration (Figure S6a in the Supporting InformationI), the collection samples with lower concentrations were more prone to random error in matching the blank between the standards and samples due to their higher f_B.

DOI: 10.1021/acs.est.7b00592
Environ. Sci. Technol. 2017, 51, 6268−6278

Consequently, for accurate δ^{15}N-NO analyses, soil NO should be collected to achieve >3 μM NO_2^- + NO_3^- in the solution within 2 h (equivalent to collecting a flow of >26 ppbv NO over a 2 h period). Blank 20% TEA solution should then be used to dilute both soil NO collection samples and isotopic standards within a batch to a common concentration for injection of 10 nmol of N using the denitrifier method. Control tests using a soil NO sample collected from the laboratory rewetting experiment (δ^{15}N = −37.1‰, [NO_2^-] + [NO_3^-] = 9.2 μM) indicate that dilution-induced uncertainty in the δ^{15}N was <0.5‰ for a dilution up to 3-fold but still giving >3 μM NO_2^- + NO_3^- in the solution (data not shown). This uncertainty is within the analytical uncertainty (i.e., ±0.8‰ for RSIL20). Therefore, we always group samples with similar concentrations such that the dilution factor does not exceed 3.

Overall, our intercalibration effort demonstrates that although the NO recovery was slightly less than 100%, fractionation during chamber mixing and NO conversion and collection was effectively minimized under the tested conditions. The derived standard deviation of ±1.1‰ based on all the collection samples with an average P_{diff} of ±7% (i.e., the sample peak area is within 100% ± 7% of that of RSIL20) represents the overall accuracy and precision across the entire method, accounting for propagated errors from the total N blank and its mismatch between the standards and samples. While the method precision is lower than that of the modified EPA method (Table S1 in the Supporting Information), our integrated method featuring simultaneous NO flux measurement and collection is the first to show its suitability for unbiased soil δ^{15}N-NO determination under realistic, varying soil conditions. Furthermore, the method is more convenient than previous methods and does not require time-consuming pretreatments for δ^{15}N analysis (Table S1 in the Supporting Information). Given the good result from the intercalibration, the tank NO can be utilized as a secondary standard for correcting the isobaric interference. For instance, the tank NO can be collected before and after soil NO collection; Δ^{17}O of the tank collection samples can then be estimated using an empirical relationship scaling a 1‰ increase from the accepted δ^{15}N value (−71.4‰ in this case) to every 18.8‰ increase in Δ^{17}O to correct the soil collection samples.[86]

Application to Pulsed Soil NO Emissions. Pulsed NO emission was triggered by soil rewetting under both the laboratory and field conditions (Figure 4). In the laboratory, the pulsed NO emission was temporally variable, with a rapid initial NO pulse being triggered upon the rewetting (Figure 4a). While the initial NO pulse was absent under the field conditions, possibly due to the relatively high prewetting soil water content (0.17 $cm^3 \cdot cm^{-3}$), the rewetting and N amendments caused significantly increased NO emission as compared to the prewetting emission (47 ± 16 $nmol \cdot m^{-2} \cdot min^{-1}$). Particularly, a dramatic increase in NO emission was triggered by the NO_2^- addition (Figure 4b).

Twenty and fifteen samples were collected for the δ^{15}N-NO analysis from the laboratory and field experiments, respectively (Tables S5 and S6 in the Supporting Information). The average NO recovery was 102.2% ± 5.6% and 108.6% ± 11.0% for the laboratory and field collection samples, respectively. The >100% recovery was detected mostly in samples collected with the NO_2^- addition (NO recovery 117.5% ± 11.6%; Table S6 in the Supporting Information). We suspect that the >100% NO recovery might result from our underestimation of the soil NO emission due to the slow response time of the chemiluminescent analyzer (>30 s), especially given that transient fluctuations in the NO flux were likely triggered by the NO_2^- addition (Figure 4b). Alternatively, the >100% recovery could result from soil emission of NO_y (NO_y = NO_2 + HONO + HNO_3 + other non-NO reactive nitrogen oxides),[87] which can potentially be collected in the TEA solution as NO_2^- and/or NO_3^-.[65] If soil NO_y emission were significant during measurement, it would be detected as NO_2 by our chemiluminescent analyzer with a molybdenum convertor.[88] Because the NO_2 flux never exceed 2% of the simultaneous NO flux (Figures S11 and S12 in the Supporting Information), contributions of NO_y emission to the NO recovery and the measured δ^{15}N-NO are considered negligible. Future application of the DFC-TEA method can be coupled to a faster NO measurement system along with existing denuder and wet chemistry methods[76,89] that quantitatively scrub NO_y without significant loss of NO.

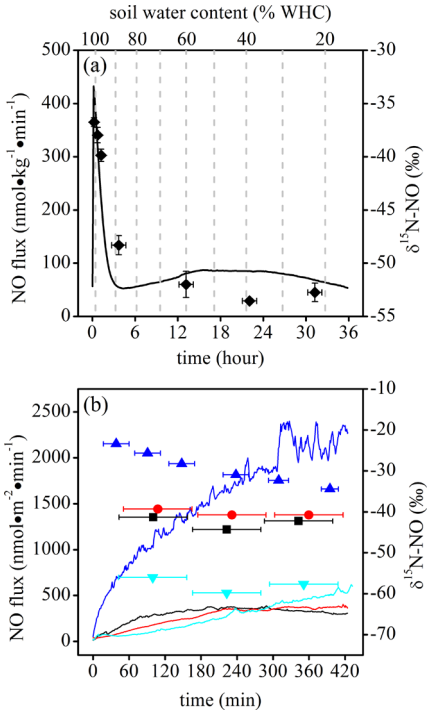

Figure 4. NO emission (lines) and δ^{15}N-NO (dots) results from the laboratory (a) and field (b) rewetting experiments. The error bar on the *x*-axis denotes the time span of each collection sample. In the field rewetting experiment, four soil plots were respectively wetted on four consecutive days using 500 mL of Milli-Q water (black), 20 mM KNO_3 (red; δ^{15}N = 46.5‰ ± 0.3‰), 10 mM $NaNO_2$ (dark blue; δ^{15}N = 1.0‰ ± 0.4‰), and 20 mM NH_4Cl (light blue; δ^{15}N = 1.7‰ ± 0.1‰) solutions.

The measured soil δ^{15}N-NO exhibited intriguing patterns that are indicative of mechanisms underlying the soil NO emissions (Figure 4). In the laboratory rewetting of the air-dried soil samples, the initial NO pulse had higher δ^{15}N values (−36.7‰ to −39.9‰) than NO emission after 12 h of postwetting (−52.0‰ to −53.6‰; Figure 4a). Recent work by Homyak et al.[33] provided evidence that, in arid soils, abiotic reactions govern the rapid initial NO pulse, whereas microbial processes control later emissions as microbes recover from drought stress. Therefore, the higher δ^{15}N-NO values associated with the initial NO pulse may suggest that abiotic reactions likely bear a smaller isotopic fractionation on NO production than microbial processes. However, the temporal

DOI: 10.1021/acs.est.7b00592
Environ. Sci. Technol. 2017, 51, 6268−6278

variation of δ^{15}N-NO could also result from changing rates of microbial NO production[90] or sequential resuscitation of different microbial groups[91] during the rewetting. Further constraints on the relevant isotope effects are needed to tease apart the relative importance of abiotic and microbial pathways sustaining pulsed NO emissions in soils. In the field rewetting experiment where an initial NO pulse was lacking, the measured soil δ^{15}N-NO responded differently to the added N precursors (Figure 4b). First, the δ^{15}N-NO values that evolved from the NH_4^+ (−59.8‰ to −56.0‰) and NO_2^- (−34.4‰ to −23.4‰) amendments were significantly lower and higher relative to the control (Milli-Q water addition; −44.3‰ to −41.3‰), respectively, in spite of the almost equal δ^{15}N of the added NH_4^+ and NO_2^-. Second, despite the high δ^{15}N of the added NO_3^- (i.e., 46.5‰), the δ^{15}N-NO values measured from the NO_3^- amendment (−40.7‰ to −39.4‰) were not significantly different from those in the control. The measured soil δ^{15}N-NO and its differential responses to the amended N sources indicate that various soil NO-producing processes (e.g., nitrification, denitrification, and chemodenitrification), stimulated by different N amendments, likely bear distinguishable isotopic imprints on NO production, similar to what has been observed in soil nitrous oxide (N_2O) studies.[37−39] For example, N_2O production in soil was found to be associated with a larger isotope effect for nitrification of NH_4^+ (e.g., −45‰ to −67‰) than denitrification of NO_2^- (e.g., −35‰ to −22‰).[37−39] Thus, soil δ^{15}N-NO measurement could potentially provide important implications for understanding couplings between soil NO and N_2O emissions, in that NO is the precursor of N_2O in most abiotic and microbial processes.[10,17−20] Finally, the measured soil δ^{15}N-NO values are significantly lower than those of other measured NO_x emission sources,[44,45,47−49] confirming the use of soil δ^{15}N-NO as a robust tracer of regional N deposition.[41,42] Quantification of isotope effects associated with NO dynamics in soils therefore represents an important avenue for future research on the soil−atmosphere cycling of reactive N.

■ ASSOCIATED CONTENT

Supporting Information

The Supporting Information is available free of charge on the ACS Publications website at DOI: 10.1021/acs.est.7b00592.

Comparison between the DFC-TEA method and previously published NO_x collection methods, description of the dynamic flux chamber system, protocol for NO_2^- and NO_3^- concentration measurement using the modified spongy cadmium reduction method, total N blank and the blank-matching strategy, extended modeling of the NO conversion in excess O_3, calculation of the theoretical Δ^{17}O value of the NO_2 produced from the NO + O_3 reaction, experimental setup of the field rewetting experiment, soil NO_y emissions in the laboratory and field soil rewetting experiments, and complete data sets of the laboratory and field collection samples (PDF)

■ AUTHOR INFORMATION

Corresponding Author

*Phone: 973-718 0238; fax: 412-624 8780; e-mail: zhy35@pitt.edu.

ORCID

Zhongjie Yu: 0000-0002-4935-0154

Notes

The authors declare no competing financial interest.

■ ACKNOWLEDGMENTS

This material is based upon work supported by a National Science Foundation CAREER award (Grant No. 1253000) to E.M.E. We thank Kathrine Redling, Vivian Feng, Madeline Ellgass, and Madeline Gray for assistance with the isotopic measurements.

■ REFERENCES

(1) *Climate Change 2013: The Physical Science Basis*; Contribution of Working Group I to the Fifth Assessment Report of the Intergovernmental Panel on Climate Change; Cambridge University Press: Cambridge, U.K., 2013.

(2) Richter, A.; Burrows, J. P.; Nüß, H.; Granier, C.; Niemeier, U. Increase in tropospheric nitrogen dioxide over China observed from space. *Nature* **2005**, *437* (7055), 129−132.

(3) Jacob, D. J.; Heikes, E. G.; Fan, S. M.; Logan, J. A.; Mauzerall, D. L.; Bradshaw, J. D.; Singh, H. B.; Gregory, G. L.; Talbot, R. W.; Blake, D. R.; Sachse, G. W. Origin of ozone and NO_x in the tropical troposphere: A photochemical analysis of aircraft observations over the South Atlantic basin. *J. Geophys. Res. Atmos.* **1996**, *101* (D19), 24235−24250.

(4) Jang, M.; Czoschke, N. M.; Lee, S.; Kamens, R. M. Heterogeneous atmospheric aerosol production by acid-catalyzed particle-phase reactions. *Science* **2002**, *298* (5594), 814−817.

(5) Likens, G. E.; Driscoll, C. T.; Buso, D. C. Long-term effects of acid rain: response and recovery of a forest ecosystem. *Science* **1996**, *272* (5259), 244.

(6) Akimoto, H. Global air quality and pollution. *Science* **2003**, *302* (5651), 1716−1719.

(7) Jaeglé, L.; Steinberger, L.; Martin, R. V.; Chance, K. Global partitioning of NO_x sources using satellite observations: Relative roles of fossil fuel combustion, biomass burning and soil emissions. *Faraday Discuss.* **2005**, *130*, 407−423.

(8) Zhang, R.; Tie, X.; Bond, D. W. Impacts of anthropogenic and natural NO_x sources over the US on tropospheric chemistry. *Proc. Natl. Acad. Sci. U. S. A.* **2003**, *100* (4), 1505−1509.

(9) Galbally, I. E.; Roy, C. R. Loss of fixed nitrogen from soils by nitric oxide exhalation. *Nature* **1978**, *275*, 734−735.

(10) Skiba, U.; Smith, K. A.; Fowler, D. Nitrification and denitrification as sources of nitric oxide and nitrous oxide in a sandy loam soil. *Soil Biol. Biochem.* **1993**, *25* (11), 1527−1536.

(11) Yienger, J. J.; Levy, H. Empirical model of global soil-biogenic NO_x emissions. *J. Geophys. Res.* **1995**, *100* (D6), 11447−11464.

(12) Bertram, T. H.; Heckel, A.; Richter, A.; Burrows, J. P.; Cohen, R. C. Satellite measurements of daily variations in soil NO_x emissions. *Geophys. Res. Lett.* **2005**, *32* (24), L24812.

(13) Hudman, R. C.; Russell, A. R.; Valin, L. C.; Cohen, R. C. Interannual variability in soil nitric oxide emissions over the United States as viewed from space. *Atmos. Chem. Phys.* **2010**, *10* (20), 9943−9952.

(14) Steinkamp, J.; Lawrence, M. G. Improvement and evaluation of simulated global biogenic soil NO emissions in an AC-GCM. *Atmos. Chem. Phys.* **2011**, *11* (12), 6063−6082.

(15) Vinken, G. C. M.; Boersma, K. F.; Maasakkers, J. D.; Adon, M.; Martin, R. V. Worldwide biogenic soil NO_x emissions inferred from OMI NO_2 observations. *Atmos. Chem. Phys.* **2014**, *14* (18), 10363−10381.

(16) Steinkamp, J.; Ganzeveld, L. N.; Wilcke, W.; Lawrence, M. G. Influence of modelled soil biogenic NO emissions on related trace gases and the atmospheric oxidizing efficiency. *Atmos. Chem. Phys.* **2009**, *9* (8), 2663−2677.

(17) Zumft, W. G. Cell biology and molecular basis of denitrification. *Microbiol. Mol. Biol. Rev.* **1997**, *61* (4), 533−616.

(18) Kester, R. A.; De Boer, W.; Laanbroek, H. J. Production of NO and N_2O by Pure Cultures of Nitrifying and Denitrifying Bacteria

DOI: 10.1021/acs.est.7b00592
Environ. Sci. Technol. 2017, 51, 6268−6278

during Changes in Aeration. *Appl. Environ. Microbiol.* **1997**, *63* (10), 3872−3877.
(19) Firestone, M. K.; Davidson, E. A. Microbiological basis of NO and N_2O production and consumption in soil. In *Exchange of Trace Gases between Terrestrial Ecosystems and the Atmosphere*; Andreae, M. O., Schimel, D. S., Robertson, G. P., Eds.; John Wiley & Sons Ltd.: Berlin, 1989; pp 7−21.
(20) Venterea, R. T.; Rolston, D. E. Nitric and nitrous oxide emissions following fertilizer application to agricultural soil: Biotic and abiotic mechanisms and kinetics. *J. Geophys. Res. Atoms.* **2000**, *105* (D12), 15117−15129.
(21) McCalley, C. K.; Sparks, J. P. Abiotic gas formation drives nitrogen loss from a desert ecosystem. *Science* **2009**, *326* (5954), 837−840.
(22) Homyak, P. M.; Kamiyama, M.; Sickman, J. O.; Schimel, J. P. Acidity and organic matter promote abiotic nitric oxide production in drying soils. *Global Change Biol.* **2017**, *23* (4), 1735−1747.
(23) Yang, W. X.; Meixner, F. X. Laboratory studies on the release of nitric oxide from sub-tropical grassland soils: The effect of soil temperature and moisture. In *Gaseous Nitrogen Emissions from Grasslands*; Jarvis, S. C., Pain, B. F., Eds.; Centre for Agriculture and Bioscience International (CABI): Wallingford, U.K., 1997; pp 67−71.
(24) Van Dijk, S. M.; Gut, A.; Kirkman, G. A.; Gomes, B. M.; Meixner, F. X.; Andreae, M. O. Biogenic NO emissions from forest and pasture soils: Relating laboratory studies to field measurements. *J. Geophys. Res.* **2002**, *107* (D20), 8058.
(25) Hall, S. J.; Matson, P. A. Nitrogen oxide emissions after nitrogen additions in tropical forests. *Nature* **1999**, *400* (6740), 152−155.
(26) Davidson, E. A.; Keller, M.; Erickson, H. E.; Verchot, L. V.; Veldkamp, E. Testing a Conceptual Model of Soil Emissions of Nitrous and Nitric Oxides. *BioScience* **2000**, *50* (8), 667−680.
(27) Davidson, E. A.; Verchot, L. V. Testing the Hole-in-the-Pipe Model of nitric and nitrous oxide emissions from soils using the TRAGNET database. *Global Biogeochem. Cycles* **2000**, *14* (4), 1035−1043.
(28) Hudman, R. C.; Moore, N. E.; Mebust, A. K.; Martin, R. V.; Russell, A. R.; Valin, L. C.; Cohen, R. C. Steps towards a mechanistic model of global soil nitric oxide emissions: implementation and space based-constraints. *Atmos. Chem. Phys.* **2012**, *12* (16), 7779−7795.
(29) Jaeglé, L.; Martin, R. V.; Chance, K.; Steinberger, L.; Kurosu, T. P.; Jacob, D. J.; Modi, A. I.; Yoboué, V.; Sigha-Nkamdjou, L.; Galy-Lacaux, C. Satellite mapping of rain-induced nitric oxide emissions from soils. *J. Geophys. Res. Atmos.* **2004**, *109* (D21), D21310.
(30) Oikawa, P. Y.; Ge, C.; Wang, J.; Eberwein, J. R.; Liang, L. L.; Allsman, L. A.; Grantz, D. A.; Jenerette, G. D. Unusually high soil nitrogen oxide emissions influence air quality in a high-temperature agricultural region. *Nat. Commun.* **2015**, *6*, 8753.
(31) Davidson, E. A. Sources of nitric oxide and nitrous oxide following wetting of dry soil. *Soil Sci. Soc. Am. J.* **1992**, *56* (1), 95−102.
(32) Davidson, E. A. Pulses of nitric oxide and nitrous oxide flux following wetting of dry soil: An assessment of probable sources and importance relative to annual fluxes. *Ecol. Bull.* **1992**, 149−155.
(33) Homyak, P. M.; Blankinship, J. C.; Marchus, K.; Lucero, D. M.; Sickman, J. O.; Schimel, J. P. Aridity and plant uptake interact to make dryland soils hotspots for nitric oxide (NO) emissions. *Proc. Natl. Acad. Sci. U. S. A.* **2016**, *113* (19), E2608−E2616.
(34) Wang, Y.; McElroy, M. B.; Martin, R. V.; Streets, D. G.; Zhang, Q.; Fu, T. M. Seasonal variability of NO_x emissions over east China constrained by satellite observations: Implications for combustion and microbial sources. *J. Geophys. Res.* **2007**, *112* (D6), D06301.
(35) Hudman, R. C.; Jacob, D. J.; Turquety, S.; Leibensperger, E. M.; Murray, L. T.; Wu, S.; Gilliland, A. B.; Avery, M.; Bertram, T. H.; Brune, W.; Cohen, R. C.; Dibb, J. E.; Flocke, F. M.; Fried, A.; Holloway, J.; Neuman, J. A.; Orville, R.; Perring, A.; Ren, X.; Sachse, G. W.; Singh, H. B.; Swanson, A.; Wooldridge, P. J. Surface and lightning sources of nitrogen oxides over the United States: Magnitudes, chemical evolution, and outflow. *J. Geophys. Res.* **2007**, *112* (D12), D12S05.
(36) Denk, T. R.; Mohn, J.; Decock, C.; Lewicka-Szczebak, D.; Harris, E.; Butterbach-Bahl, K.; Kiese, R.; Wolf, B. The nitrogen cycle: A review of isotope effects and isotope modeling approaches. *Soil Biol. Biochem.* **2017**, *105*, 121−137.
(37) Mariotti, A.; Germon, J. C.; Hubert, P.; Kaiser, P.; Letolle, R.; Tardieux, A.; Tardieux, P. Experimental determination of nitrogen kinetic isotope fractionation: some principles; illustration for the denitrification and nitrification processes. *Plant Soil* **1981**, *62* (3), 413−430.
(38) Sutka, R. L.; Ostrom, N. E.; Ostrom, P. H.; Breznak, J. A.; Gandhi, H.; Pitt, A. J.; Li, F. Distinguishing nitrous oxide production from nitrification and denitrification on the basis of isotopomer abundances. *Appl. Environ. Microbio.* **2006**, *72* (1), 638−644.
(39) Park, S.; Pérez, T.; Boering, K. A.; Trumbore, S. E.; Gil, J.; Marquina, S.; Tyler, S. C. Can N_2O stable isotopes and isotopomers be useful tools to characterize sources and microbial pathways of N_2O production and consumption in tropical soils? *Global Biogeochem. Cycles* **2011**, *25* (1), GB1001.
(40) Hastings, M. G.; Casciotti, K. L.; Elliott, E. M. Stable isotopes as tracers of anthropogenic nitrogen sources, deposition, and impacts. *Elements* **2013**, *9* (5), 339−344.
(41) Elliott, E. M.; Kendall, C.; Wankel, S. D.; Burns, D. A.; Boyer, E. W.; Harlin, K.; Bain, D. J.; Butler, T. J. Nitrogen isotopes as indicators of NO_x source contributions to atmospheric nitrate deposition across the midwestern and northeastern United States. *Environ. Sci. Technol.* **2007**, *41* (22), 7661−7667.
(42) Elliott, E. M.; Kendall, C.; Boyer, E. W.; Burns, D. A.; Lear, G. G.; Golden, H. E.; Harlin, K.; Bytnerowicz, A.; Butler, T. J.; Glatz, R. Dual nitrate isotopes in dry deposition: Utility for partitioning NO_x source contributions to landscape nitrogen deposition. *J. Geophys. Res.* **2009**, *114* (G4), G04020.
(43) Hastings, M. G.; Jarvis, J. C.; Steig, E. J. Anthropogenic impacts on nitrogen isotopes of ice-core nitrate. *Science* **2009**, *324* (5932), 1288−1288.
(44) Felix, J. D.; Elliott, E. M.; Shaw, S. L. Nitrogen isotopic composition of coal-fired power plant NO_x: influence of emission controls and implications for global emission inventories. *Environ. Sci. Technol.* **2012**, *46* (6), 3528−3535.
(45) Redling, K.; Elliott, E.; Bain, D.; Sherwell, J. Highway contributions to reactive nitrogen deposition: tracing the fate of vehicular NO_x using stable isotopes and plant biomonitors. *Biogeochemistry* **2013**, *116* (1−3), 261−274.
(46) Hoering, T. The isotopic composition of the ammonia and the nitrate ion in rain. *Geochim. Cosmochim. Acta* **1957**, *12* (1), 97−102.
(47) Walters, W. W.; Goodwin, S. R.; Michalski, G. Nitrogen stable isotope composition ($\delta^{15}N$) of vehicle-emitted NO_x. *Environ. Sci. Technol.* **2015**, *49* (4), 2278−2285.
(48) Walters, W. W.; Tharp, B. D.; Fang, H.; Kozak, B. J.; Michalski, G. Nitrogen isotope composition of thermally produced NO_x from various fossil-fuel combustion sources. *Environ. Sci. Technol.* **2015**, *49* (19), 11363−11371.
(49) Fibiger, D. L.; Hastings, M. G. First measurements of the nitrogen isotopic composition of NO_x from biomass burning. *Environ. Sci. Technol.* **2016**, *50* (21), 11569−11574.
(50) Li, D.; Wang, X. Nitrogen isotopic signature of soil-released nitric oxide (NO) after fertilizer application. *Atmos. Environ.* **2008**, *42* (19), 4747−4754.
(51) Felix, J. D.; Elliott, E. M. The agricultural history of human-nitrogen interactions as recorded in ice core $\delta^{15}N\text{-}NO_3^-$. *Geophys. Res. Lett.* **2013**, *40* (8), 1642−1646.
(52) Felix, J. D.; Elliott, E. M. Isotopic composition of passively collected nitrogen dioxide emissions: Vehicle, soil and livestock source signatures. *Atmos. Environ.* **2014**, *92*, 359−366.
(53) Hutchinson, G. L.; Yang, W. X.; Andre, C. E. Overcoming humidity dependence of the chromium trioxide converter used in luminol-based nitric oxide detection. *Atmos. Environ.* **1998**, *33* (1), 141−145.

DOI: 10.1021/acs.est.7b00592
Environ. Sci. Technol. 2017, 51, 6268−6278

(54) Robinson, J. K.; Bollinger, M. J.; Birks, J. W. Luminol/H_2O_2 chemiluminescence detector for the analysis of nitric oxide in exhaled breath. *Anal. Chem.* **1999**, *71* (22), 5131−5136.
(55) Fibiger, D. L.; Hastings, M. G.; Lew, A. F.; Peltier, R. E. Collection of NO and NO_2 for isotopic analysis of NO_x emissions. *Anal. Chem.* **2014**, *86* (24), 12115−12121.
(56) Wojtal, P. K.; Miller, D. J.; O'Conner, M.; Clark, S. C.; Hastings, M. G. Automated, high-resolution mobile collection system for the nitrogen isotopic analysis of NO_x. *J. Visualized Exp.* **2016**, *118*, e54962.
(57) Pape, L.; Ammann, C.; Nyfeler-Brunner, A.; Spirig, C.; Hens, K.; Meixner, F. X. An automated dynamic chamber system for surface exchange measurement of non-reactive and reactive trace gases of grassland ecosystems. *Biogeosciences* **2009**, *6* (3), 405−429.
(58) Yu, Z.; Slater, L. D.; Schäfer, K. V.; Reeve, A. S.; Varner, R. K. Dynamics of methane ebullition from a peat monolith revealed from a dynamic flux chamber system. *J. Geophys. Res.: Biogeosci.* **2014**, *119* (9), 1789−1806.
(59) Miyazaki, K.; Matsumoto, J.; Kato, S.; Kajii, Y. Development of atmospheric NO analyzer by using a laser-induced fluorescence NO_2 detector. *Atmos. Environ.* **2008**, *42* (33), 7812−7820.
(60) Hargrove, J.; Zhang, J. Measurements of NO_x, acyl peroxynitrates, and NO_y with automatic interference corrections using a NO_2 analyzer and gas phase titration. *Rev. Sci. Instrum.* **2008**, *79* (4), 046109−046109.
(61) Fuchs, H.; Dubé, W. P.; Lerner, B. M.; Wagner, N. L.; Williams, E. J.; Brown, S. S. A sensitive and versatile detector for atmospheric NO_2 and NO_x based on blue diode laser cavity ring-down spectroscopy. *Environ. Sci. Technol.* **2009**, *43* (20), 7831−7836.
(62) Wild, R. J.; Edwards, P. M.; Dubé, W. P.; Baumann, K.; Edgerton, E. S.; Quinn, P. K.; Roberts, J. M.; Rollins, A. W.; Veres, P. R.; Warneke, C.; Williams, E. J.; Yuan, B.; Brown, S. S. A Measurement of Total Reactive Nitrogen, NO_y, together with NO_2, NO, and O_3 via Cavity Ring-down Spectroscopy. *Environ. Sci. Technol.* **2014**, *48* (16), 9609−9615.
(63) Wagner, N. L.; Dubé, W. P.; Washenfelder, R. A.; Young, C. J.; Pollack, I. B.; Ryerson, T. B.; Brown, S. S. Diode laser-based cavity ring-down instrument for NO3, N2O5, NO, NO2 and O3 from aircraft. *Atmos. Meas. Tech.* **2011**, *4* (6), 1227−1240.
(64) Glasius, M.; Funch Carlsen, M.; Stroyer Hansen, T.; Lohse, C. Measurements of nitrogen dioxide on Funen using diffusion tubes. *Atmos. Environ.* **1999**, *33* (8), 1177−1185.
(65) Cape, J. N. The use of passive diffusion tubes for measuring concentrations of nitrogen dioxide in air. *Crit. Rev. Anal. Chem.* **2009**, *39* (4), 289−310.
(66) Wei, Y.; Oshima, M.; Simon, J.; Motomizu, S. The application of the chromatomembrane cell for the absorptive sampling of nitrogen dioxide followed by continuous determination of nitrite using a micro-flow injection system. *Talanta* **2002**, *57* (2), 355−364.
(67) Jones, M. N. Nitrate reduction by shaking with cadmium: alternative to cadmium columns. *Water Res.* **1984**, *18* (5), 643−646.
(68) Sigman, D. M.; Casciotti, K. L.; Andreani, M.; Barford, C.; Galanter, M. B. J. K.; Böhlke, J. K. A bacterial method for the nitrogen isotopic analysis of nitrate in seawater and freshwater. *Anal. Chem.* **2001**, *73* (17), 4145−4153.
(69) Casciotti, K. L.; Sigman, D. M.; Hastings, M. G.; Böhlke, J. K.; Hilkert, A. Measurement of the oxygen isotopic composition of nitrate in seawater and freshwater using the denitrifier method. *Anal. Chem.* **2002**, *74* (19), 4905−4912.
(70) Casciotti, K. L.; Böhlke, J. K.; McIlvin, M. R.; Mroczkowski, S. J.; Hannon, J. E. Oxygen isotopes in nitrite: analysis, calibration, and equilibration. *Anal. Chem.* **2007**, *79* (6), 2427−2436.
(71) McIlvin, M. R.; Casciotti, K. L. Technical updates to the bacterial method for nitrate isotopic analyses. *Anal. Chem.* **2011**, *83* (5), 1850−1856.
(72) Michalski, G.; Savarino, J.; Böhlke, J. K.; Thiemens, M. Determination of the total oxygen isotopic composition of nitrate and the calibration of a $\Delta^{17}O$ nitrate reference material. *Anal. Chem.* **2002**, *74* (19), 4989−4993.
(73) Kaiser, J.; Hastings, M. G.; Houlton, B. Z.; Röckmann, T.; Sigman, D. M. Triple oxygen isotope analysis of nitrate using the denitrifier method and thermal decomposition of N_2O. *Anal. Chem.* **2007**, *79* (2), 599−607.
(74) Su, H.; Cheng, Y.; Oswald, R.; Behrendt, T.; Trebs, I.; Meixner, F. X.; Andreae, M. O.; Cheng, P.; Zhang, Y.; Pöschl, U. Soil nitrite as a source of atmospheric HONO and OH radicals. *Science* **2011**, *333* (6049), 1616−1618.
(75) Oswald, R.; Behrendt, T.; Ermel, M.; Wu, D.; Su, H.; Cheng, Y.; Breuninger, C.; Moravek, A.; Mougin, E.; Delon, C.; Loubet, B.; Pommerening-Roser, A.; Sorgel, M.; Poschl, U.; Hoffmann, T.; Andreae, M. O.; Meixner, F. X.; Trebs, I. HONO emissions from soil bacteria as a major source of atmospheric reactive nitrogen. *Science* **2013**, *341* (6151), 1233−1235.
(76) Zhou, X.; Qiao, H.; Deng, G.; Civerolo, K. A method for the measurement of atmospheric HONO based on DNPH derivatization and HPLC analysis. *Environ. Sci. Technol.* **1999**, *33* (20), 3672−3679.
(77) *Method 7—Determination of Nitrogen Oxide Emissions from Stationary Sources*; U.S. Environmental Protection Agency: Washington, DC, 1996. www3.epa.gov/ttn/emc/promgate/m-07.pdf.
(78) Michalski, G.; Kolanowski, M.; Riha, K. M. Oxygen and nitrogen isotopic composition of nitrate in commercial fertilizers, nitric acid, and reagent salts. *Isot. Environ. Health Stud.* **2015**, *51* (3), 382−391.
(79) Altieri, K. E.; Hastings, M. G.; Peters, A. J.; Oleynik, S.; Sigman, D. M. Isotopic evidence for a marine ammonium source in rainwater at Bermuda. *Glob. Biogeochem. Cycles* **2014**, *28* (10), 1066−1080.
(80) *Chemical Kinetics and Photochemical Data for Use in Atmospheric Studies Evaluation Number 15*; Jet Propulsion Laboratory, National Aeronautics and Space Administration: Pasadena, CA, 2006. https://trs.jpl.nasa.gov/handle/2014/41648.
(81) Dubé, W. P.; Brown, S. S.; Osthoff, H. D.; Nunley, M. R.; Ciciora, S. J.; Paris, M. W.; McLaughlin, R. J.; Ravishankara, A. R. Aircraft instrument for simultaneous, in situ measurement of NO_3 and N_2O_5 via pulsed cavity ring-down spectroscopy. *Rev. Sci. Instrum.* **2006**, *77* (3), 034101.
(82) Atkinson, R.; Arey, J. Gas-phase tropospheric chemistry of biogenic volatile organic compounds: a review. *Atmos. Environ.* **2003**, *37*, 197−219.
(83) Atkinson, R.; Baulch, D. L.; Cox, R. A.; Crowley, J. N.; Hampson, R. F.; Hynes, R. G.; Jenkin, M. E.; Rossi, M. J.; Troe, J.; IUPAC Subcommitte. Evaluated kinetic and photochemical data for atmospheric chemistry: Volume II−gas phase reactions of organic species. *Atmos. Chem. Phys.* **2006**, *6* (11), 3625−4055 10.5194/acp-6-3625-2006.
(84) Dahal, B.; Hastings, M. G. Technical considerations for the use of passive samplers to quantify the isotopic composition of NO_x and NO_2 using the denitrifier method. *Atmos. Environ.* **2016**, *143*, 60−66.
(85) Riemer, N.; Vogel, H.; Vogel, B.; Anttila, T.; Kiendler-Scharr, A.; Mentel, T. F. Relative importance of organic coatings for the heterogeneous hydrolysis of N_2O_5 during summer in Europe. *J. Geophys. Res.* **2009**, *114* (D17), D17307.
(86) Coplen, T. B.; Böhlke, J. K.; Casciotti, K. L. Using dual-bacterial denitrification to improve $\delta^{15}N$ determinations of nitrates containing mass-independent ^{17}O. *Rapid Commun. Mass Spectrom.* **2004**, *18* (3), 245−250.
(87) Soper, F. M.; Boutton, T. W.; Groffman, P. M.; Sparks, J. P. Nitrogen trace gas fluxes from a semiarid subtropical savanna under woody legume encroachment. *Global Biogeochem. Cycles* **2016**, *30* (5), 614−628.
(88) Dunlea, E. J.; Herndon, S. C.; Nelson, D. D.; Volkamer, R. M.; San Martini, F.; Sheehy, P. M.; Zahniser, M. S.; Shorter, J. H.; Wormhoudt, J. C.; Lamb, B. K.; Allwine, E. J.; Gaffney, J. S.; Marley, N. A.; Grutter, M.; Marquez, C.; Blanco, S.; Cardenas, B.; Retama, A.; Ramos Villegas, C. R.; Kolb, C. E.; Molina, L. T.; Molina, M. J. Evaluation of nitrogen dioxide chemiluminescence monitors in a polluted urban environment. *Atmos. Chem. Phys.* **2007**, *7* (10), 2691−2704.
(89) De Santis, F.; Allegrini, I.; Di Filippo, P.; Pasella, D. Simultaneous determination of nitrogen dioxide and peroxyacetyl

DOI: 10.1021/acs.est.7b00592
Environ. Sci. Technol. 2017, 51, 6268−6278

nitrate in ambient atmosphere by carbon-coated annular diffusion denuder. *Atmos. Environ.* **1996**, *30* (14), 2637−2645.
(90) Mariotti, A.; Leclerc, A.; Germon, J. C. Nitrogen isotope fractionation associated with the $NO_2^- \rightarrow N_2O$ step of denitrification in soils. *Can. J. Soil Sci.* **1982**, *62* (2), 227−241.
(91) Placella, S. A.; Brodie, E. L.; Firestone, M. K. Rainfall-induced carbon dioxide pulses result from sequential resuscitation of phylogenetically clustered microbial groups. *Proc. Natl. Acad. Sci. U. S. A.* **2012**, *109* (27), 10931−10936.

DOI: 10.1021/acs.est.7b00592
Environ. Sci. Technol. 2017, 51, 6268−6278

Supporting Information

Novel Method for Nitrogen Isotopic Analysis of Soil-Emitted Nitric Oxide

Zhongjie Yu and Emily M. Elliott*

University of Pittsburgh, Department of Geology and Environmental Science, Pittsburgh, PA 15260, USA

* Corresponding author. Phone: (973) 718 0238; fax: (412) 624 8780; Email: zhy35@pitt.edu

41 pages, 12 Figures, 6 Tables

Table of contents

S1. Comparison between the developed method and previously published NO_x collection method.

Table S1. Comparisons of the DFC-TEA method with other published methods for NO_x collection and isotopic analysis.

Characteristics	modified EPA method[1-3]	Fibiger method[4-6]	Li and Wang method[7]	DFC-TEA method
Collection setup	bulk air sample is sucked into pre-evacuated gas sampling bulb containing NO_2 trapping solution	sample flow is forced to pass through a NO_x-trapping bubbler	sample flow is forced to pass through a NO-NO_2 convertor and then a NO_2-trapping denuder	sample flow is forced to pass through a NO-NO_2 convertor and then a NO_2-trapping bubbler
NO-NO_2 conversion	NO is oxidized by ambient-level O_2 to NO_2	NO and NO_2 are directly collected and oxidized to NO_3^- in $KMnO_4$/NaOH solution	solid oxidizer consisting of granules impregnated with CrO_3/H_3PO_4	excess O_3
NO_2 collection	H_2SO_4/H_2O_2 solution		denuder coated with KOH/guaiacol solution	20% triethanolamine solution
NO_x recovery	>97.5%	100±5%	100% (inferred from breakthrough test)	98.5±3.5%
NO_x concentration tested	tens to hundreds of ppmv	22 – 1070 ppbv	5 ppmv	9 – 749 ppbv
Reagent N blank	not reported	5 – 7 µM	not reported	~0.12 µM
Sample pre-treatment for isotopic analysis	sampling bulb needs to stand for at least 72 h for NO oxidation and NO_2 trapping; the absorbing solution is then collected and neutralized using 1 M $NaHCO_3$	$KMnO_4$ is removed through reduction with H_2O_2 to MnO_2 precipitate; the MnO_2 precipitate is removed from solution by centrifugation and decanting; after decanting, the solution is neutralized using 12 N HCl.	denuder is eluted with methanol and water; the elute is first dried in a vacuum desiccator and then collected in tin boats.	solution is neutralized using 12 N HCl
Isotopic analysis	denitrifier method (NO_3^- conversion to N_2O) coupled to IRMS	denitrifier method (NO_3^- conversion to N_2O) coupled to IRMS	online combustion (NO_2^- conversion to N_2) coupled to IRMS	denitrifier method (NO_3^- /NO_2^- conversion to N_2O) coupled to IRMS
Isotopic calibration	certified NO_3^- standards	certified NO_3^- standards	a standard reagent ($\delta^{15}N$ =	certified NO_3^- and NO_2^-

Characteristics	modified EPA method[1-3]	Fibiger method[4-6]	Li and Wang method[7]	DFC-TEA method
			0.4‰)	(δ^{15}N = -79.6‰) standards
Precision	better than ±0.5‰	±1.5‰	±0.3‰	±1.1‰
Inter-calibration	not conducted	not conducted	reference NO tank used for the method evaluation was directly measured by a GC-IRMS; agreed within 0.2‰	inter-calibrated with the modified EPA method; agreed within 0.3‰
Minimum NO_2^-/NO_3^- concentration required in collection media	not available	>2 μM (calculated through error propagation assuming a sample δ^{15}N-NO_x not very different from blank δ^{15}N-NO_3^-, e.g., δ^{15}N-NO_x=0.5‰)[5]	not available	>3 μM (experimentally determined using a reference NO tank with low δ^{15}N-NO, i.e., δ^{15}N-NO= -71.4‰)
Temperature and relative humidity effects	not relevant	not relevant	not tested; NO conversion and collection are potentially severely interfered by variations in relative humidity of sample flow.	tested; no significant effect under tested laboratory and field conditions
Tested interference	ammonia	ammonia	not reported	ammonia, nitrous acid (indirectly)
Laboratory application	not applied	coupled to smog chambers for δ^{15}N-NO_x measurements of diesel engine emissions and biomass burning	coupled to a closed non-steady-state chamber for δ^{15}N-NO measurements of fertilization-induced NO emission in agricultural soils	coupled to a dynamic steady-state chamber system for δ^{15}N-NO measurements of rewetting-induced soil NO pulses
Field application	δ^{15}N-NO_x of vehicular tailpipe exhausts	coupled to a mobile platform for δ^{15}N-NO_x measurement of on-road vehicular exhaust plume	not applied	coupled to a dynamic steady-state chamber system for δ^{15}N-NO measurements of rewetting- and N fertilization-induced soil NO pulses

S2. Supplementary description of the DFC system

S2.1 Flux calculation

The DFC is a technique that has been developed to continuously measure soil-atmosphere fluxes of various compounds including NO.[8, 9] In contrast to closed static chambers, the DFC is designed to maintain a constant flow of outside air through the chamber containing soil samples or enclosing soil surface areas of interest. The gas flux at the soil-air boundary layer is then determined by the mass balance in the enclosed headspace as following,[10]

$$V \times \frac{M_N}{V_m} \times \frac{d\mu_{\text{cham}}}{dt} = A \times F - Q \times (\mu_{\text{cham}} - \mu_{\text{in}}) \times \frac{M_N}{V_m} \qquad \text{Equation S1}$$

where t denotes time; V is the chamber volume; Q is the flow rate of the chamber purging flow; A is the surface area enclosed by the chamber or the mass of incubated soil samples in the chamber; μ_{cham} and μ_{in} are the gas mixing ratios of the purging inflow and the outflowing chamber air, respectively. M_N/V_m is the conversion factor (i.e., ppbv to ng·m^{-3}), where M_N is the gas molecular weight and V_m is the molar volume at measured temperature in the chamber headspace and assumed pressure of 1 atm. When the system operates under a steady state with zero air being the purging flow, $d\mu_{\text{cham}}/dt = 0$ in Eq. 1, and the mass budget equation can be reduced and rearranged to:[10]

$$F = \frac{Q}{A} \times \mu_{\text{cham}} \times \frac{M_N}{V_m} \qquad \text{Equation S2}$$

Importantly, by using Eq. S2 to measure soil NO flux, it assumes that (1) the chamber headspace is completely mixed, such that NO concentration (μ_{cham}) is uniform throughout the chamber headspace and (2) NO behaves conservatively, so that there are no reactions with other air constituents or with the chamber walls.[10]

In the developed DFC system, zero air free of NO_x and O_3 is produced in the air purification unit (Figure 1 in the main text) up to 20 slpm for purging the flux chamber. NO, NO_2, and ammonia (NH_3) concentrations in the chamber headspace are measured alternately by a chemiluminescent analyzer (Model 17i, Thermo Fisher Scientific) at 10 s intervals for flux calculations. The precision of NO, NO_2, and NH_3 measurements are ±0.4 ppbv, ±0.6 ppbv, and ±0.6 ppbv, respectively.

S2.2 Fabrication and testing of the field chamber

A field soil flux chamber has been fabricated and tested for its suitability for NO flux and δ^{15}N-NO measurements, following considerations suggested by Pape et al.[10] and Yu et al.[11] The chamber consists of a cylindrical flow-through chamber (39 cm I.D. and 30 L inner volume) made of 5 mm thick transparent acrylic plastic (Figure S1). The chamber interior surface was lined with 0.05 mm thick FEP film (DuPont, USA) to enhance chemical resistance to NO.[10] During field soil flux measurements, the chamber is fitted to the top of a stainless steel chamber base inserted 10 cm into soil (Figure S1a). A rubber gasket and twelve wing nuts are used to obtain a gas-tight seal for the chamber closure. For testing the chamber in the laboratory, the chamber base was replaced by a stainless steel sheet (Figure S1b). Soil temperature, air temperature and relative humidity of the chamber atmosphere are continuously monitored using two HOBO sensors installed through the chamber ceiling and sealed with plugs (Figure S1).

Because soil gas effluxes are driven both by diffusion and mass flow, with diffusion being controlled by gas concentration gradient and mass flow by pressure gradient at soil surface,[12] accurate soil gas flux measurements using a DFC require careful system design to eliminate artifacts and biases in measured fluxes. As can be seen in Eq. S2, when the soil gas flux (F) is positive (net emission to the atmosphere) and constant, the gas concentration in the

chamber headspace (μ_{cham}) is inversely related to the purging flow rate (Q) under steady state. In this sense, a large purging flow rate that prevents prolonged accumulation of measured gas is desirable for maintaining an undisturbed gas concentration gradient at the soil-chamber air interface. On the other hand, however, if the purging flow rate is too large, the chamber headspace is artificially pressurized, resulting in higher-than-ambient chamber pressures and, consequently, suppressed mass flows from enclosed soils.

In our field DFC system, we used a purging flow rate between 5 slpm and 20 slpm, corresponding to a mean air residence time ($\tau_{cham}=V/Q$) ranging from 1.5 to 6.0 minutes under complete mixing conditions. This range of τ_{cham} falls within the middle range reported in the literature (see Table 4 in Pape et al.[10] for a summary) and is considered a compromise between minimizing disturbance on pressure and concentration gradients. In addition, the outflow duct of the chamber (2 inch I.D.) is enlarged compared to the inflow duct (1 inch I.D.) to reduce the purging-induced pressure buildup inside the chamber[10] and covered by a stainless steel wind shield to prevent episodic pressure change triggered by horizontal wind blowing (Figure S1).[13] The pressure difference between the chamber headspace and the ambient atmosphere is then estimated to be at the lower range as reported in the literature, less than a few Pa, because, as stated above, the resistance at the chamber outlet is effectively minimized and the applied purging flow rate is common (see Table S1 in Yu et al.[11] for a summary on the effects of chamber configuration on the pressure difference).

The chamber has been tested for the assumption of complete and conservative mixing inherent to flux calculation using Eq. S2. The analytical solution of the differential Eq. S1 is a first order exponential decay function depicting evolution of the gas concentration toward steady state,[10]

$$\mu_{\mathrm{cham}}(t) = \mu_{\mathrm{in}} + F \times \frac{A \times V_m}{Q \times M_N}\left(1 - e^{-\frac{t}{\tau_{cham}}}\right) \qquad \text{Equation S3}$$

Although a direct and accurate observation of this equilibration process for NO is hardly possible in our system due to the delay effects introduced by the limited response times of the chemiluminescent analyzer (>30 s), the temporal evolution of the equilibration was investigated using chamber relative humidity measurements that are recorded without any time delay. Five soil samples obtained from an urban forest, Pittsburgh, PA, (100 g dry soil per sample) wetted to 100% WFPS, were placed inside the chamber as the source of water vapor, and the chamber air temperature and relative humidity were recorded every 5 s before and after chamber closure (Figure S1b).

Figure S2a shows the temporal buildup of water vapor concentration in the chamber under continuous purging of ambient laboratory air at 5 slpm and 20 slpm. These rates correspond to a theoretical τ_{cham} of 6.0 min and 1.5 min, respectively, under the experimental condition. An exponential fit to the measured water vapor concentration yielded a τ_{cham} of 6.1 min and 1.7 min, respectively. The small difference between the measured and theoretical τ_{cham} values may result from uncertainties in geometric calculation of the chamber volume (V). We therefore conclude that complete mixing conditions in the chamber headspace are closely approximated when a purging flow rate between 5 slpm and 20 slpm is used.

Furthermore, we tested NO transmission from the field DFC system, because biases may be generated in NO flux and δ^{15}N-NO measurements if there are significant NO losses on the chamber wall and/or losses via reactions with other air constituents. NO transmission from the field chamber was measured and calculated by purging the chamber with a flow of

known NO concentration (μ_{in}) and subsequent measurement of NO concentration in the chamber headspace (μ_{cham}), according to Eq. S4.

$$\text{NO transimission} = \left(\frac{\mu_{\text{cham}}}{\mu_{\text{in}}}\right) \times 100 \qquad \text{Equation S4}$$

The results show that NO transmission is greater than 98.3±0.3% over the tested ranges of μ_{in} (0-100 ppbv) and chamber purging flow rate (5-20 slpm) (Fig. S2b), indicating that NO loss is insignificant in the chamber.

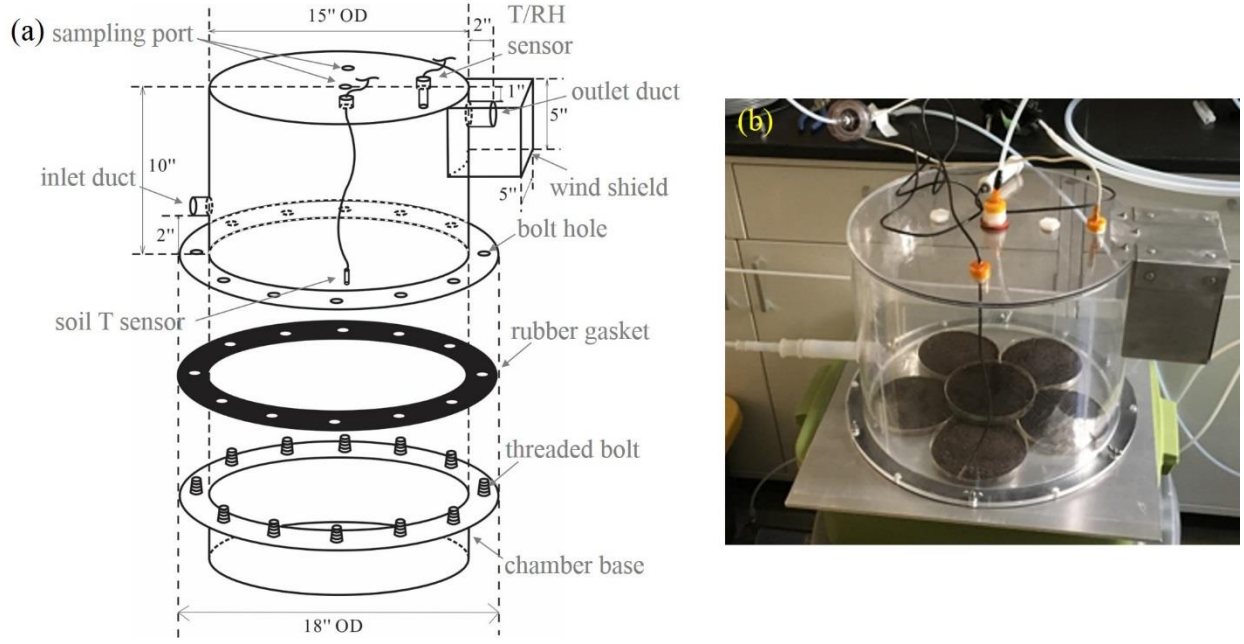

Figure S1. Schematic (a) and picture (b) of the field chamber.

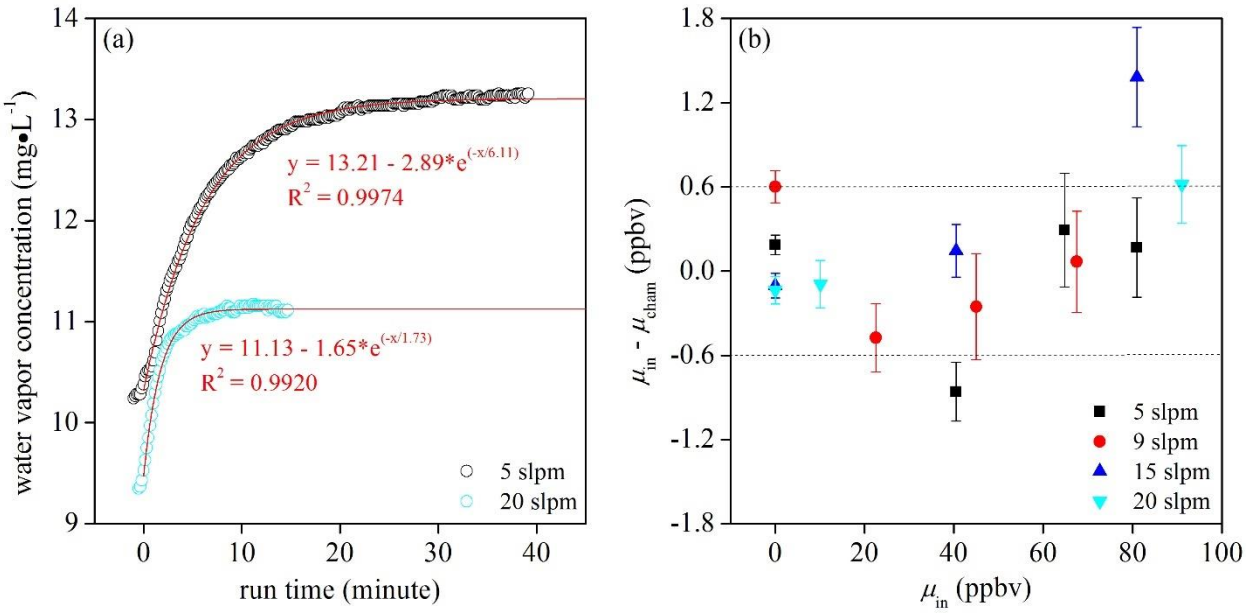

Figure S2. (a) Temporal buildup of water vapor concentration under purging of two different flow rates after wetting of soil samples in the chamber; (b) difference between μ_{in} and μ_{cham} under different μ_{in} and purging flow rates. The dashed lines bracket the uncertainty range of μ_{in} - μ_{cham} with an expected value of zero (±0.6 ppbv), propagated from the precision of NO concentration measurement (±0.4 ppbv).

S2.3 DFC system specifications

A schematic of the developed DFC system is shown in Figure 1 of the main text. Opaque 0.25 inch O.D. PTFE tubing was used to connect the entire system. Specifications of each component of the DFC system are provided in Table S2.

Table S2. Specifications of the DFC system components.

ID	Component	Description
1	Diaphragm pump	
	• Diaphragm pump for the Air purification unit	Catalog number GH-79200-00, Cole Parmer; free-air capacity = 21.2 $L \cdot min^{-1}$.
	• Diaphragm pump for the chemiluminescent analyzer	Model N026.3, KNF Neuberger.
	• Diaphragm pump for the NO collection train	Model N86 KTP, KNF Neuberger; all sample exposed parts are PTFE-coated; free-air capacity = 5.5 $L \cdot min^{-1}$.
2	Air purification columns	Three activated charcoal (catalog number NC9643579, Fisher Scientific) columns and three Purafil (catalog number NC0275433, Fisher Scientific) columns collected in series; absorbents were packed in in-line scrubber assemblies (catalog number NC0955678, Fisher Scientific); inner volume of each column = 0.5 L.
3	Drying columns	Two Dri-Rite and 5 Å molecular sieve columns connected in series (catalog number EW-01418-50, Cole Parmer); inner volume of each column = 0.5 L.
4	Humidifier	Milli-Q water in 1000 mL Pyrex gas washing bottle with plain tip stopper.
5	NO tank	50.4 ppmv NO in N_2, Matheson; purity >99.8%; analytical tolerance =±1.0%.
6	NO_2 tank	100.2 ppmv NO_2 in N_2, Matheson; analytical tolerance =±1.0%.
7	NH_3 tank	50.1 ppmv NH_3 in N_2, Matheson; analytical tolerance =±1.0%.
8	Mass flow controller	
	• Mass flow controller for the NO tank	Model SmartTrak 50, Sierra Instruments; Flow range = 0 - 50 sccm N_2; accuracy = ±1.5% full scale.
	• Mass flow controller for the NO_2 tank	Catalog number GH-32660-08, Cole Parmer; flow range = 0 -200 sccm N_2/Air; accuracy = ±1% full scale.
	• Mass flow controller for the	Catalog number GH-32660-08, Cole Parmer; flow range = 0 -200

ID	Component	Description
	NH_3 tank	sccm N_2/Air; accuracy = ±1% full scale.
	• Mass flow controller for the zero air for the laboratory DFC system	Model SmartTrak 50, Sierra Instruments; Flow range = 0 - 10 slpm Air; accuracy = ±1.5% full scale.
	• Mass flow controller for the zero air for the field DFC system	Model SmartTrak 50, Sierra Instruments; Flow range = 0 - 50 slpm Air; accuracy = ±1.5% full scale.
	• Mass flow controller for the NO collection train	Model SmartTrak 50, Sierra Instruments; Flow range = 0 - 5 slpm Air; accuracy = ±1.5% full scale.
9	Flux chamber	1000 mL standard jar made of PFA (Part 100-1000-01, Savillex) fitted with a PFA transfer closure (Part 600-110-28, Savillex). See text S1.1 for the information about the field DFC chamber.
10	Temperature and relative humidity sensor	Model RHT50, Extech Instruments; non-sensing exterior parts of the sensor was wrapped by FEP tape (catalog number 7562A13, McMaster-Carr) to enhance chemical resistance to the measured gas species.
11	In-line PTFE particulate filter assembly	Zylon membrane disc filter (pore size 5 μm, diameter = 47 mm, Part number P4PH047, Pall Corporation) secured by an in-line filter holder (part number 1119, Pall Corporation).
12	HONO scrubber	250 mL fritted gas washing bottle (LG-3761-102, Wilmad-LabGlass) containing 50 mL of 1 mM phosphate buffer solution at pH 7.0 (Zhou et al., 1999).
13	Moisture exchanger	Model ME-110-48COMP-4, Perma Pure LLC. In cases where condensing condition is encountered in the chamber, the flow is reduced in water vapor concentration before entering the NO collection train by being equilibrated with ambient air.
14	Reaction tube	PTFE tubing (catalog number 5239K15, McMaster-Carr), length 240 cm, I.D. 9.5 mm, wrapped by aluminum foil to prevent light penetration.
15	Gas washing bottle containing TEA solution	500 mL fritted gas washing bottle (LG-3761-104, Wilmad-LabGlass) containing 70 mL of 20% (v/v) triethanolamine solution; the fritted stopper of the gas washing bottle was lengthened to be just above the bottom of the bottle, and this resulted in using 70 mL of the solution to just cover the frit.
16	ozone generator	Model 146i, Thermo Fisher Scientific.
17	NO-NO_x-NH_3 chemiluminescent analyzer	Model 17i, Thermo Fisher Scientific.

S3. Protocol of NO_2^- and NO_3^- measurement using the modified spongy cadmium reduction method

Both NO_2^- and NO_3^- are produced from the reaction between NO_2 and TEA. To measure NO_2^- +NO_3^- concentration in the TEA collection samples, a few modifications were made to the spongy cadmium method.[14] Because sample pH affects the NO_3^- reduction to NO_2^- and subsequent color development for the colorimetric NO_2^- determination,[14] fresh and spent 20% TEA solutions were titrated with 12 N HCl and 85% H_3PO_4, respectively, to guide the pH adjustment (Figure S3).

To measure NO_2^-+NO_3^- concentration of the TEA collection samples, 5 mL of each sample is pipetted into a 15 mL Falcon tube. 100 μL of 12 N HCl is added to each sample to neutralize the pH to ~8.2 (Figure S3). 0.2 g wet spongy cadmium, generated from the single displacement reaction between zinc metal sticks and 20% (w/v) $CdSO_4$ solution, is then added to each sample to initiate the NO_3^- to NO_2^- reduction. The sample tubes are capped and secured in a rack on a mechanical shaker so that the tubes are horizontal for maximum mixing. The samples are shaken at 100 excursions·min^{-1} for 2 h. After the shaking, 4 mL of reduced sample is transferred into a new 15 mL Falcon tube. 160 μL of nitrite color reagent (0.05 g N-(1-naphthyl)-ethylenediamine dihydrochloride, 0.5 g Sulfanilamide, 5 mL of 85% H_3PO_4 in 45 mL of MilliQ water) and 480 μL of 85% H_3PO_4 are then added to each sample. The addition of 85% H_3PO_4 lowers the sample pH to ~3.0 and allows maximum color development. The sample tubes are immediately capped, flipped over three times, and allowed to sit for 10 min for color development. The sample absorbance at 540 nm is then measured within 10 min on a UV-visible spectrophotometer. NO_2^- concentration in the TEA collection samples is measured using the

same protocol without the cadmium reduction step. Long-term average of the absorbance value of a 10 μM NO_2^- in 20% TEA solution is about 0.3.

Control tests using 10 μM NO_2^- or NO_3^- in 20% TEA solution (n=4) indicate that 2 h shaking time gave complete NO_3^- reduction, but did not cause overreduction of NO_2^- originally present in the solution (Figure S4). Repeated measurements of a 10 μM NO_2^- or NO_3^- standard in 20% TEA (n=8) indicate that the precision (1 σ) of the method is ±0.09 μM and ±0.36 μM for NO_2^- and NO_3^-, respectively. Due to the multiple reduction and neutralization steps involved in the spongy cadmium reduction method, NO_2^- and NO_3^- standards were always prepared in 20% TEA solution for calibrating the TEA collection samples.

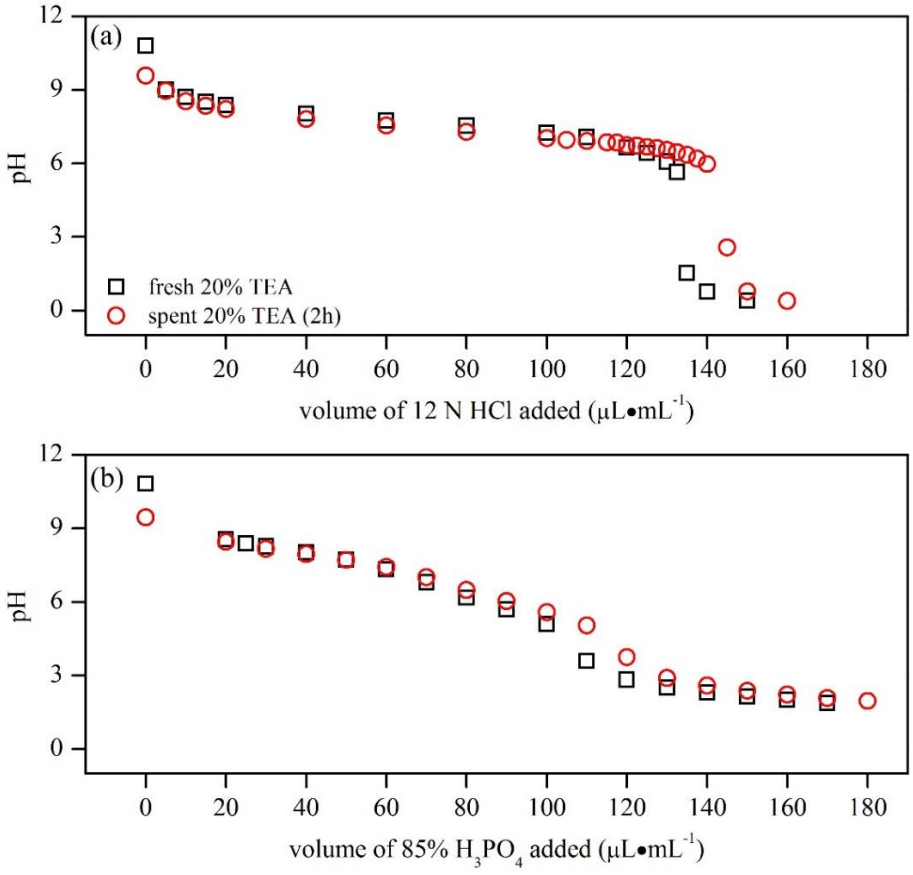

Figure S3. Titration of fresh and spent 20% TEA solution with 12 N HCl (a) and 85% H_3PO_4 (b).

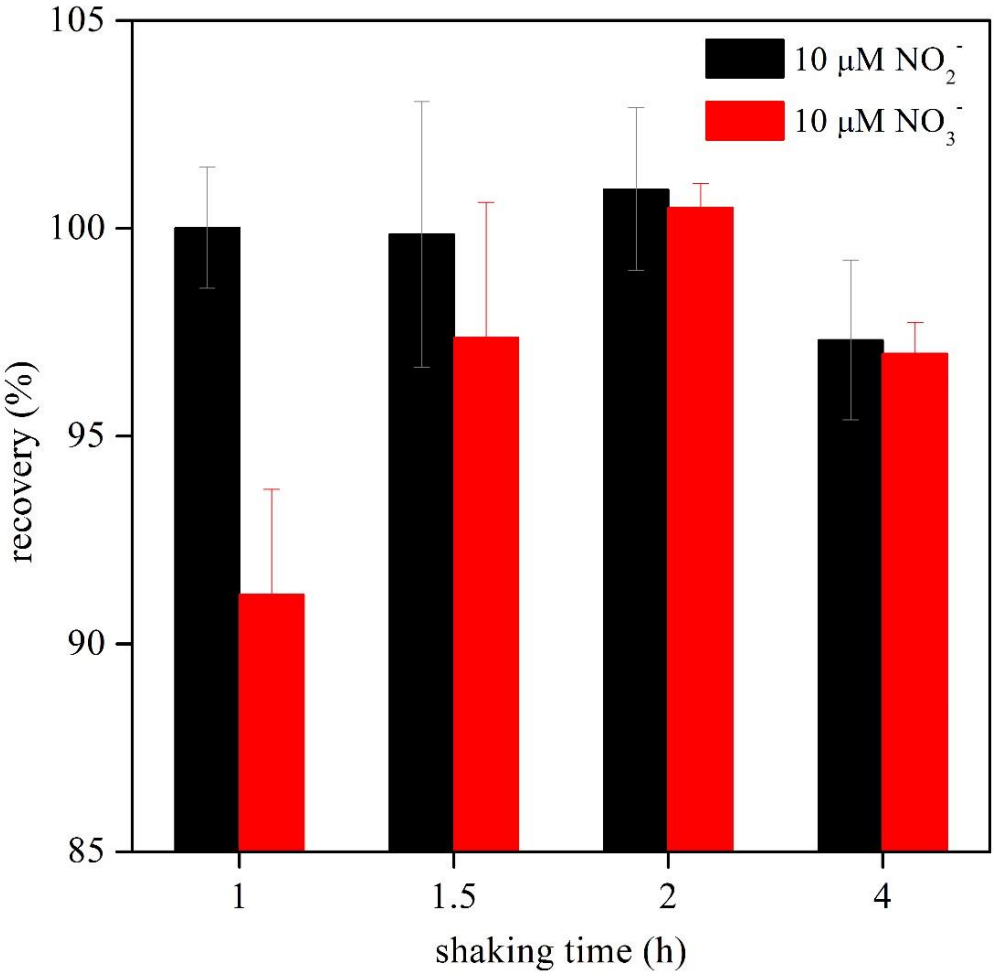

179

180 **Figure S4. Effect of shaking time on the NO_3^- reduction and the NO_2^- recovery in the**

181 **spongy cadmium reduction method.**

182

S4. The total N blank and the blank-matching strategy.

We investigated the blank size associated with the 20% TEA solution through analysis of both deionized water and blank 20% TEA solution using the denitrified method. As shown in Figure S5, injecting deionized water to the sample vials led to N_2O-N yield. This indicates a N blank inherent in the denitrifier medium.[15, 16] Higher N_2O-N yield resulting from the injections of blank 20% TEA solution indicates the N blank specific to the 20% TEA solution. The N blank of the 20% TEA solution was calculated by subtracting the N blank originating from the denitrifier medium from the total N blank and was estimated to be 0.12±0.04 μM.

The total N blank associated with the $\delta^{15}N$ analysis of the TEA collection samples using the denitrifier method (i.e., TEA N blank + blank N associated with the denitrifier medium) was also assessed independently through quantifying shrinkage of the N isotope-ratio scale between USGS34 and RSIL20 measured in each run of the TEA collection samples.[17]

$$f_B = 1 - \frac{\left(\frac{1+\delta^{15}N_{RSIL20\_m}\times 1000}{1+\delta^{15}N_{USGS34\_m}\times 1000}\right)-1}{\left(\frac{1+\delta^{15}N_{RSIL20\_a}\times 1000}{1+\delta^{15}N_{USGS34\_a}\times 1000}\right)-1} \quad \text{Equation S5}$$

In Equation S5, f_B is the fraction of N_2O-N derived from the total N blank; $\delta^{15}N_{RSIL20\text{-}a}$ and $\delta^{15}N_{USGS34\text{-}a}$ are the accepted $\delta^{15}N$ values of RSIL20 and USGS34 relative to N_2 in air, respectively; $\delta^{15}N_{RSIL20\text{-}m}$ and $\delta^{15}N_{USGS34\text{-}m}$ are the measured $\delta^{15}N$ values of RSIL20 and USGS34 relative to IAEA-N3, respectively. The molar amount of the total N blank, calculated as the difference between the total amount of measured N_2O-N in the sample vials and the amount of N_2O-N generated from the standards, was then determined using f_B and the known molar amount of the injected standards. The estimated f_B ranged between 0.04 and 0.18 and was significantly, positively correlated with $\delta^{15}N_{RSIL20\text{-}m}$ and the sample volume (Figure 2a in the main text). Fitting a linear equation to the molar amount of the total N blank and the sample volume

indicates that the N blank likely consisted of a constant component of 0.46±0.12 nmol and a sample volume-dependent component of 0.23±0.06 nmol·mL^{-1}, consistent with the blank size estimated by injecting blank 20% TEA solution (Figure S5).

The isotope effect of the total N blank is corrected during the $\delta^{15}N$ analysis using a blank-matching strategy (i.e., application of the identical treatment principal). As illustrated in Figure 2, the blank-matching strategy requires that isotope standards (i.e., IAEA-N3, USGS34, and RSIL20) are prepared in the same matrix (i.e., 20% TEA) as collection samples; then, concentrations of the standards and samples are adjusted via dilution by 20% TEA solution such that same injection volume (±5%) is used for all the standards and samples. Consequently, systematic error associated with the total N blank is implicitly and automatically corrected during the $\delta^{15}N$ analysis because the size and $\delta^{15}N$ value of the total N blank is matched between all the standards and samples in a given analytical run (Figure 2).

The percentage difference (P_{diff}) in the major N_2O (*m/z* 44) peak area between each collection sample (P_{sample}) and RSIL20 measured within the same batch (P_{RSIL}) is calculated to quantify how precisely the blank-matching strategy is implemented:

$$P_{diff} = \frac{P_{sample} - P_{RSIL}}{P_{RSIL}} \times 100\% \qquad \text{Equation S6}$$

The calculated P_{diff} ranged from -9.8% to 15.9% for all the collection samples, averaging 1.1±5.1% (Figure S6a). P_{diff} is not sensitive to the sample concentration (linear regression, $P>0.05$) (Figure S6a), indicating that the sample concentrations were precisely measured and diluted for the $\delta^{15}N$ analysis. No discernible relationship emerged between P_{diff} and the measured $\delta^{15}N$ values (Figure S6b).

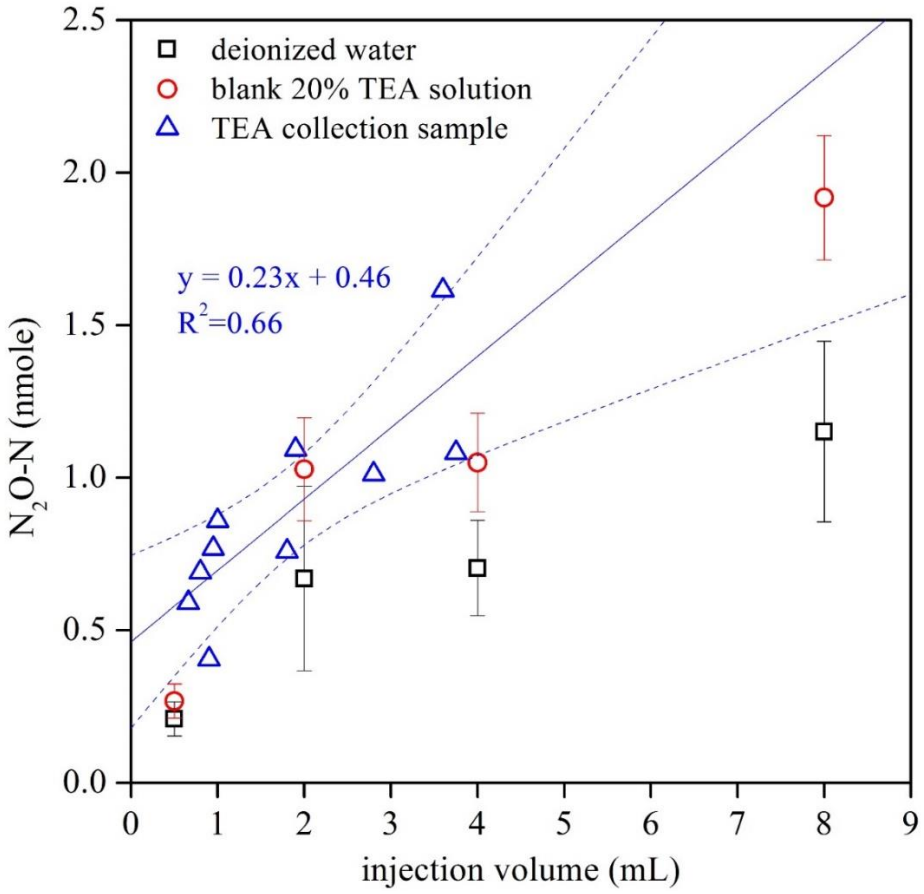

Figure S5. The N_2O-N blank associated with the bacterial medium and the 20% TEA solution as a function of the injection volume. For the injections of deionized water and blank 20% TEA solution, the N_2O-N yield was calculated from the major ion peak area, calibrating with standard additions. The solid and dashed lines denote a linear regression line and the corresponding 95% confidence interval of the N_2O-N blank associated with the TEA collection samples.

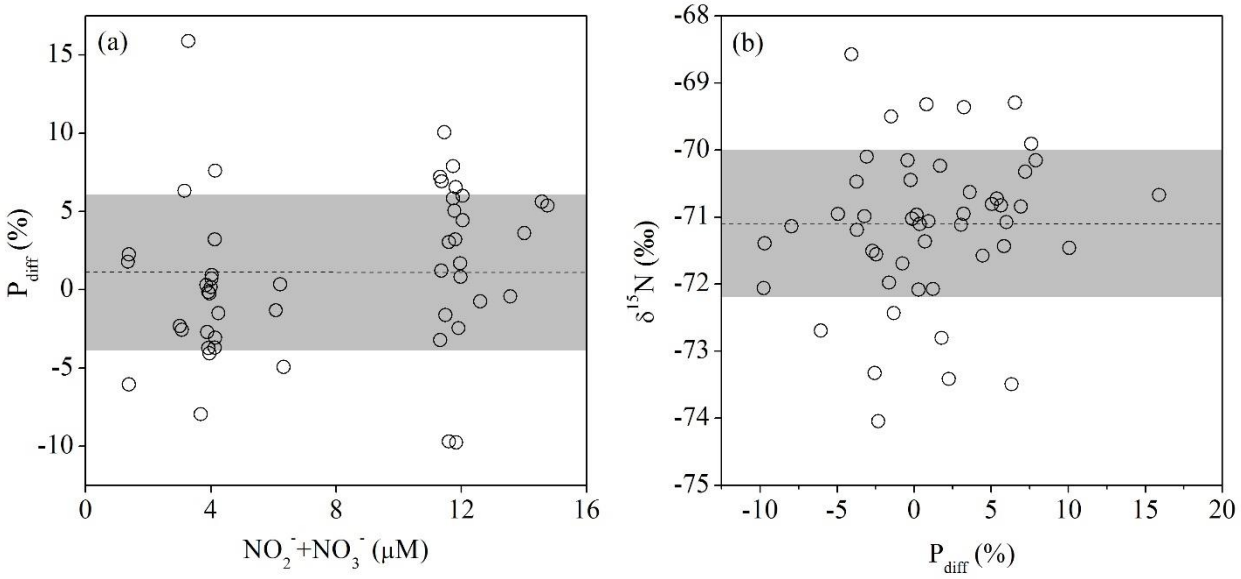

Figure S6. The calculated P_{diff} of the NO tank collection samples as a function of sample $NO_2^-+NO_3^-$ concentration (a) and its effect on the measured $\delta^{15}N$ values (b). The dash line and the shaded area represent the mean ± (1 σ) of the y-variable.

S5. Extended modeling of the NO conversion in excess O_3.

Reaction of NO with excess O_3 forms NO_2 (R1 in Table S2). In a dark environment, the efficiency of NO to NO_2 conversion is limited by the formation of higher nitrogen oxide species, i.e. nitrate radical (NO_3) and dinitrogen pentoxide (N_2O_5), from further oxidation of NO_2 (R2-R5 in Table S2). In order to model the NO conversion in the reaction tube, the reaction time is needed. Following Fuch et al.,[18] the reaction time of the reaction tube was experimentally determined by sampling zero air that contained a constant NO concentration (27 ppbv) using the NO collection train and varying the excess O_3 concentration (266-2890 ppbv). The ending point of the reaction tube was attached onto the sampling inlet of the chemiluminescent analyzer for NO concentration determination. The NO concentration decay was then fitted to a single exponential function assuming pseudo first order loss of NO in excess O_3 (Equation S7).

$$\frac{[NO]_t}{[NO]_0} = e^{(-[O_3]\times k\times t_R)} \qquad \text{Equation S7}$$

In Equation S7, $[NO]_t/[NO]_0$ is the ratio of the measured NO concentration exiting the reaction tube to the initial NO concentration; $[O_3]$ is the O_3 concentration; k is the rate constant of reaction R1; t_R is the reaction time. Due to the inner tubing of the chemiluminescent analyzer, the estimated reaction time represents the reaction tube plus the analyzer inner tubing. To correct this overestimate, the reaction time of the inner tubing was estimated by repeating the experiment with the mixing point of the sample and O_3 flow being directly attached to the analyzer inlet for NO concentration determination. The results show that the reaction time of the inner tubing of the chemiluminescent analyzer and the reaction tube plus the inner tubing were estimated to be 1.4 s and 6.4 s, respectively, with a reaction time of the reaction tube of 5 s at the measured flow temperature (22 °C) (Figure S7).

Based on this reaction time and a O_3 concentration of 2911 ppbv, numerical model calculations including reactions R1-R6 in Table S2 indicate that NO is quantitatively converted in the reaction tube and that the specific conversion of NO to NO_2 is between 98.7% and 99.0% over a wide range of NO concentrations (0-1000 ppbv) at 22 °C (Figure S8a). Notably, the remainder of the converted NO exists primarily as N_2O_5, as the efficiency of NO conversion to NO_2+N_2O_5 is always >99% under the modeled conditions (Figure S8b).

Deviations from the controlled laboratory condition could result in variations in the modeled NO conversion efficiency. Since the rate constants for reactions R1-R5 are strongly temperature-dependent, the NO conversion efficiency was further modeled over a temperature range of 0-40 °C with an assumed constant NO concentration of 100 ppbv. The result shows that deviation from the optimal temperature range (~10-20 °C) can cause a <0.5% reduction in the modeled efficiency of NO to NO_2 conversion, while the efficiency of NO conversion to NO_2+N_2O_5 is still always >99% (Figure S9). Emissions of biogenic volatile organic carbons (BVOC) from vegetated soil could potentially affect the NO conversion via reactions of BVOCs with NO_3 and O_3. The effect of BVOC emissions on the conversion efficiency was assessed by including the reactions of isoprene, a major BVOC in the atmosphere,[19] with NO_3 and O_3 in the numerical model calculation (R7 and R8 in Table S2). Interestingly, the efficiency of NO to NO_2 conversion increased by as much as 0.3% over 0 °C to 40 °C when isoprene is present at the same concentration as NO (i.e., 100 ppbv; Figure S9), possibly due to NO_3 scavenging that suppresses accumulation of N_2O_5. Therefore, it is reasonable to assume that BVOC emissions do not affect the NO conversion significantly under the applied conditions. In sum, our extended modeling on the NO conversion in excess O_3 indicates that the conversion of NO to NO_2 is not

likely to fall below 98% over a temperature range of 0-40°C in conjunction with high BVOC emissions.

Table S3. Reactions involving in the NO conversion in excess O_3.

No.	Reaction	Rate constant (at 22 °C)	Reference
R1	$NO + O_3 \rightarrow NO_2 + O_2$	1.86×10^{-14}	20
R2	$NO_2 + O_3 \rightarrow NO_3 + O_2$	2.98×10^{-17}	20
R3	$NO + NO_3 \rightarrow 2NO_2$	2.67×10^{-11}	20
R4	$NO_2 + NO_3 + M \rightarrow N_2O_5 + M$	1.19×10^{-12}	20
R5	$N_2O_5 + M \rightarrow NO_2 + NO_3 + M$	2.88×10^{-2}	20
R6	$NO_3 \rightarrow$ wall loss	2.00×10^{-1}	21
R7	$NO_3 + CH_2 = C(CH_3)CH = CH_2 \rightarrow$ products	6.86×10^{-13}	22
R8	$O_3 + CH_2 = C(CH_3)CH = CH_2 \rightarrow$ products	1.19×10^{-17}	22

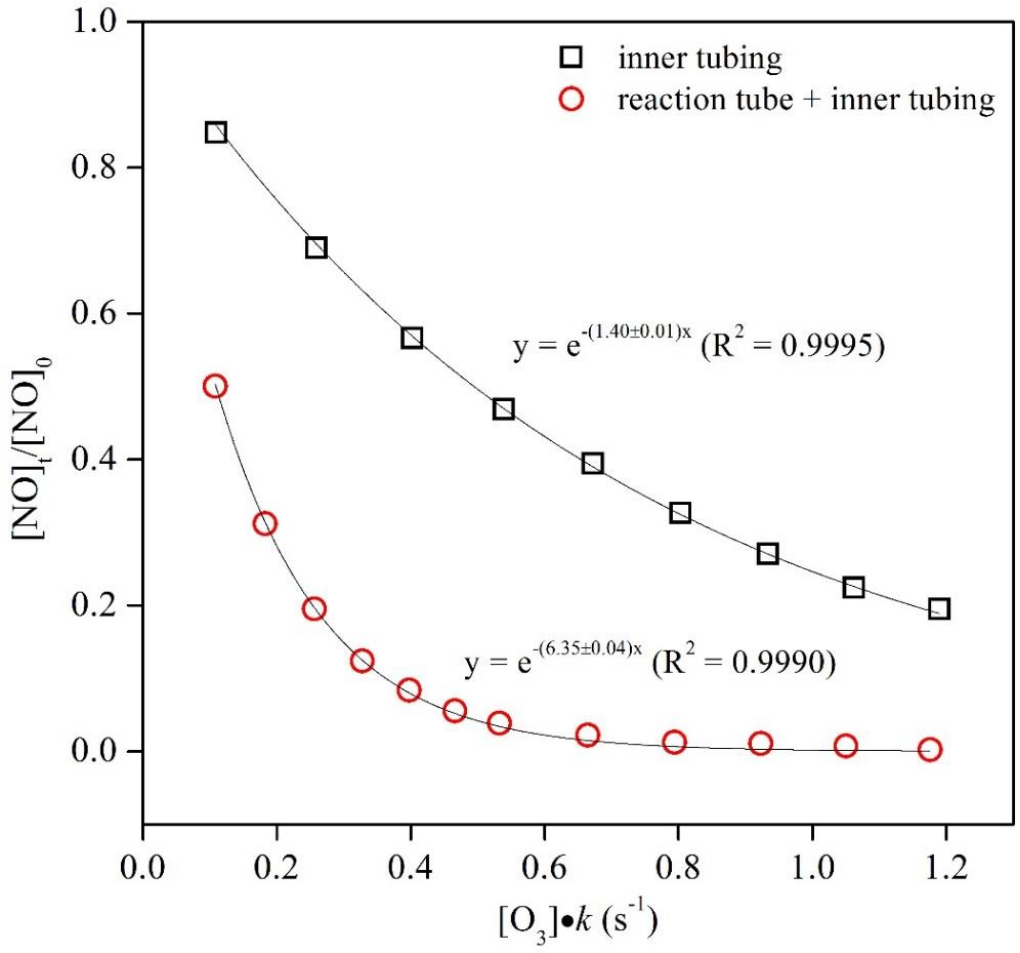

294

295 **Figure S7. Exponential fits for determining the reaction time (t_R) of the inner tubing of the**
296 **chemiluminescent analyzer and the reaction tube plus the inner tubing using Equation S7.**

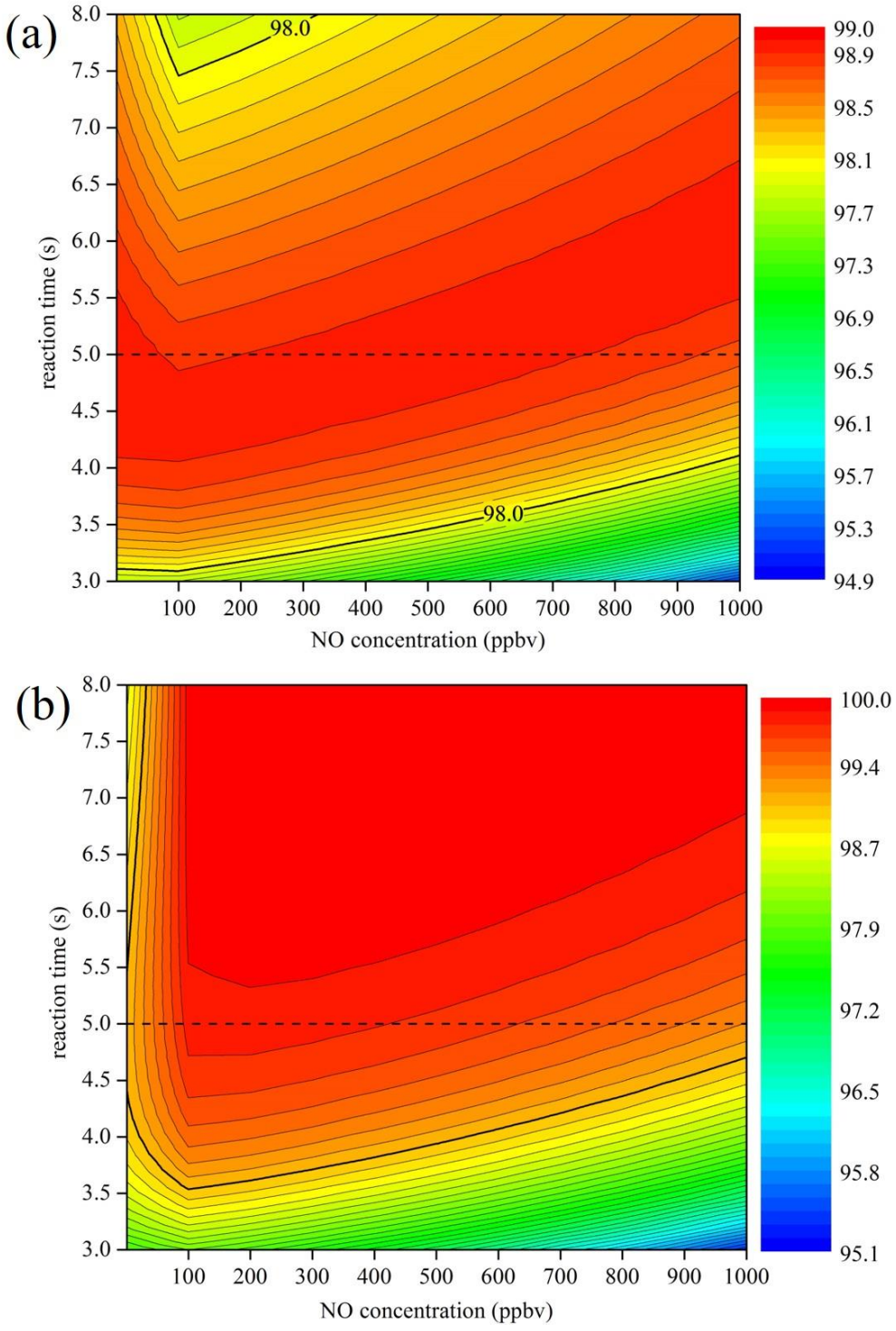

297

298 **Figure S8. Modeled efficiency of NO to NO_2 conversion (a) and NO to NO_2 + N_2O_5**
299 **conversion (b) as a function of NO concentration after the mixing of the sample and O_3**
300 **flows and the reaction time at 22 °C. The dashed line denotes the estimated reaction time (5**
301 **s) of the reaction tube.**

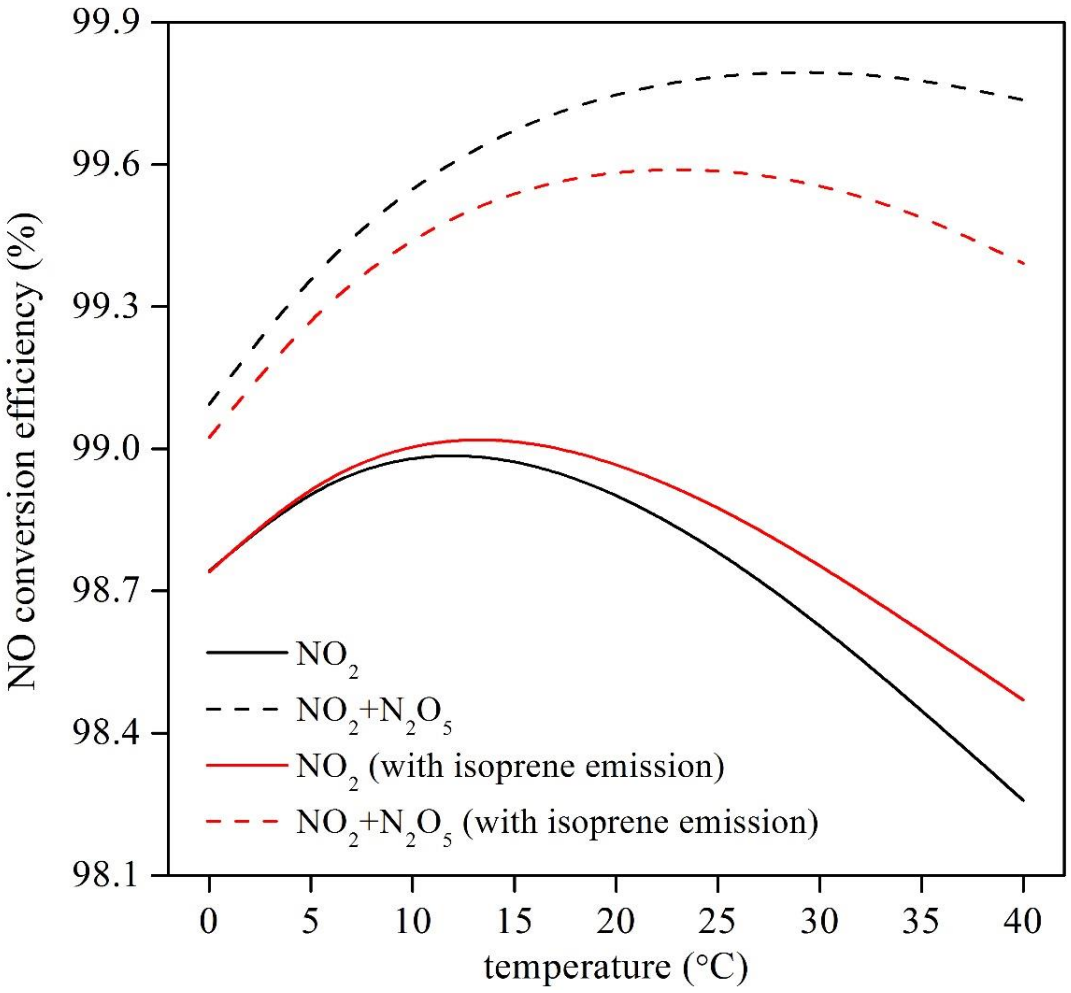

302

303 **Figure S9. Effects of temperature variation and soil isoprene emission on the modeled**
304 **efficiencies of NO conversion to NO_2 and NO_2+N_2O_5. A reaction time of 5 s and NO and**
305 **isoprene concentrations of 100 ppbv were used in the model calculations.**

S6. Determination of the theoretical $\Delta^{17}O$ of NO_2 produced from $NO+O_3$ reaction.

Positive $\Delta^{17}O$ values were observed in N_2O generated from the NO collection samples, indicating that NO_2^- and NO_3^- in the collection samples were impacted by mass-independent reactions through exchange with O_3 and that a correction of the isobaric interference on the *m/z* 45 is required. To further understand the transfer of the $\Delta^{17}O$ anomaly from O_3 during the NO conversion, we measured the $\Delta^{17}O$ of the terminal oxygen atoms of the O_3 produced from the O_3 generator on two different days by bubbling the mixed zero air and O_3 flow through a 15 µM NO_2^- solution in water for 2 h. The NO_2^- was quantitatively oxidized to NO_3^- after bubbling. The $\Delta^{17}O$ of the produced NO_3^- was measured to be 16.3±0.7‰ (n=5) and resulted in a $\Delta^{17}O$ of 48.8±2.2‰ for the terminal oxygen atoms of the produced O_3 ($\Delta^{17}O(O_3)_{trans}$). This is based on previous observations that show only the terminal atom from the O_3 molecule is abstracted in the aqueous phase NO_2^- oxidation.[23, 24]

$$NO + O_3 \rightarrow NO_2 + O_2 \qquad \text{Reaction S1}$$

Assuming that the $\Delta^{17}O$ anomaly is only located in the terminal atom[23] and that the oxygen atom transfer in reaction S1 proceeds with a probability of 8% for the abstraction of the central oxygen atom of the O_3 by NO (Equation S8),[25] the $\Delta^{17}O$ of the transferred oxygen atom ($\Delta^{17}O(O_3)_{trans}$) is calculated to be 45.0±3.7‰, equivalent to a theoretical $\Delta^{17}O$ of 22.5±1.8‰ for the NO_2 produced from reaction S1.

$$\Delta^{17}O(O_3)_{\text{trans}} = 1.18 \times \left(\frac{2}{3} \times \Delta^{17}O(O_3)_{\text{term}}\right) + 6.6 \qquad \text{Equation S8}$$

S7. Supplementary figure showing the setup of the field rewetting experiment.

Figure S10. Pictures showing (a) the University of Pittsburgh *Mobile Air Quality Laboratory*, (b) field DFC system, (c) tarp for drying urban fallow soil, and (d) field chamber.

S8. Soil NO_y emissions in the laboratory and field soil rewetting experiments.

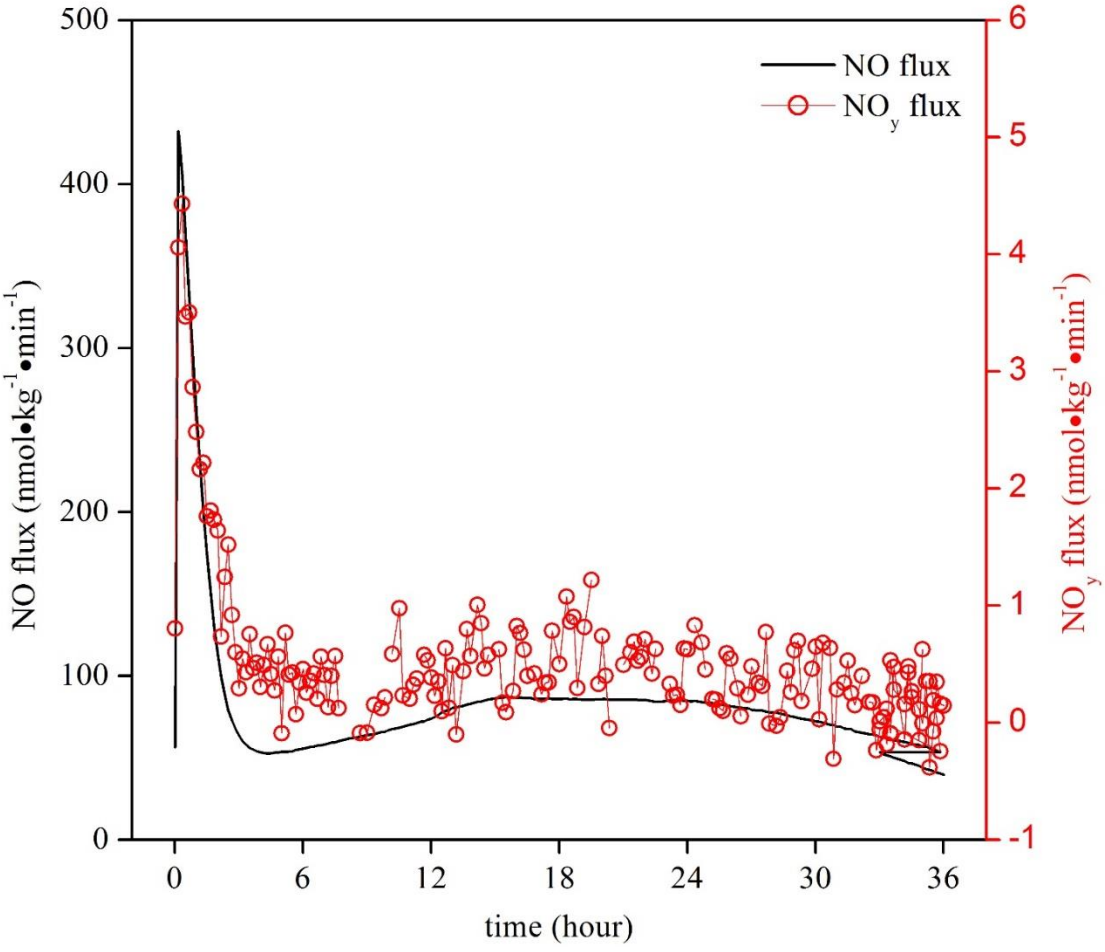

Figure S11. Soil NO and NO_y emissions in the laboratory soil rewetting experiment. Emissions were calculated based on three replicate measurements. The average ratio of NO_y flux to NO flux was 0.59±0.44%.

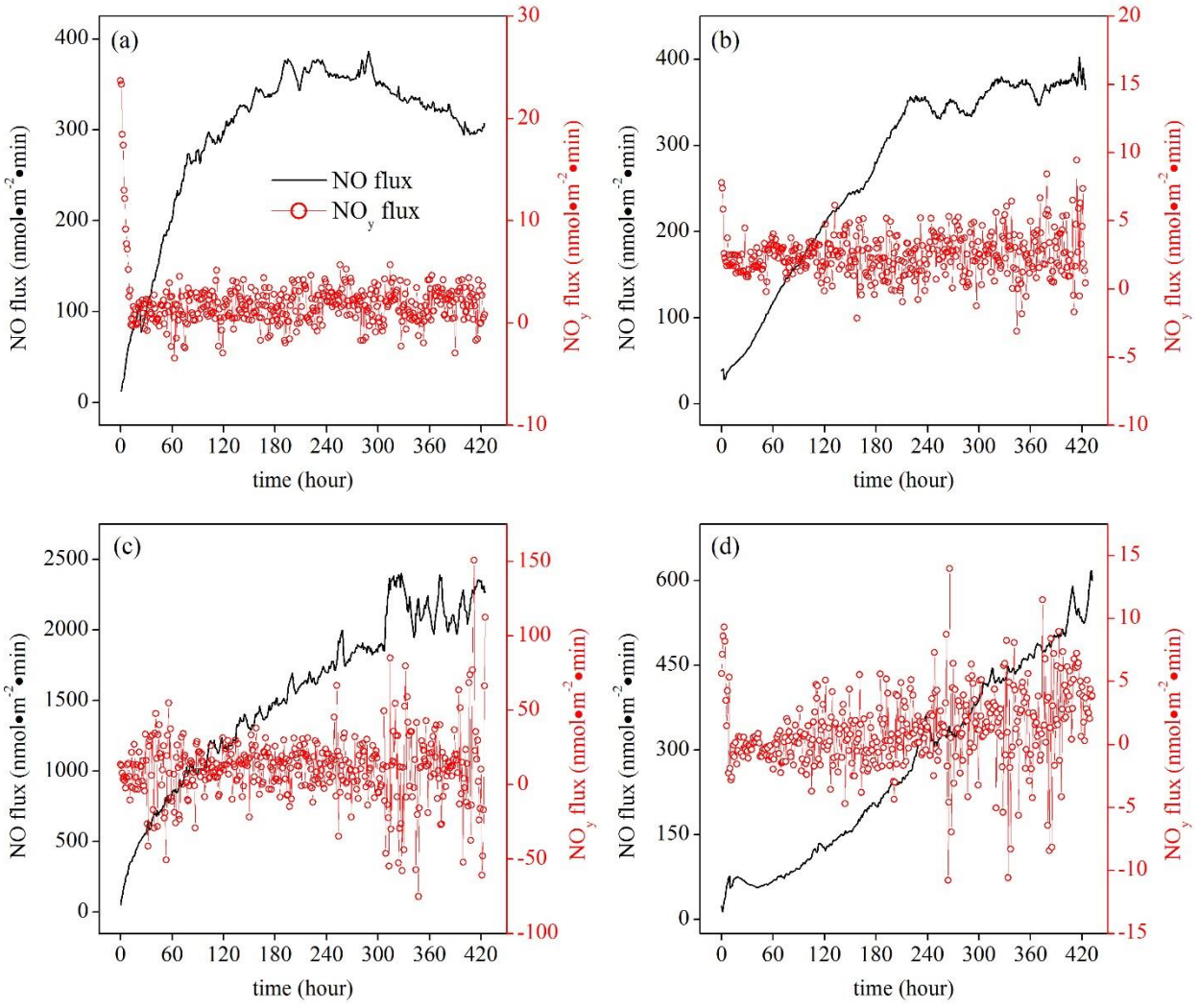

Figure S12. Soil NO and NO_y emissions in the field soil rewetting experiment. The average ratios of NO_y flux to NO flux were 0.57±0.61% for the MilliQ water addition (a), 1.14±0.99% for the NO_3^- addition (b), 0.79±1.68% for the NO_2^- addition (c), and 0.23±1.20% for the NH_4^+ addition (d). The high NO_y fluxes in the first 10 min reflect the purging out of ambient NO_2 after the chamber closure and were not included in the ratio calculations.

S9. Complete datasets for collection of NO and NO_2 reference gas tanks and pulsed NO emissions.

Table S4. Complete dataset: NO and NO_2 reference gas tanks.

Sample	Time (min)	T (°C)	RH (%)	$NO_2^-+NO_3^-$ (µM)	Recovery (%)	NO_2^- percent (%)	P_{diff} (%)	$\delta^{15}N^a$ (‰)	$\Delta^{17}O$ (‰)
NO_2 collection – laboratory DFC system									
1002 ppbv NO_2	135	23.8	25.6	125.6	96.1	87.3	6.7	-39.9	
1002 ppbv NO_2	135	23.7	25.4	133.8	102.4	87.7	-3.7	-41.1	
1002 ppbv NO_2	135	23.6	25.2	134.8	103.1	87.1	7.3	-40.9	
1002 ppbv NO_2	135	23.7	25.0	136.1	104.0	87.6	3.1	-39.6	
Mean				132.5	101.4	87.4	3.3	-40.4	
Standard error (1 σ)				4.7	3.6	0.3	5.1	0.7	
NO collection – laboratory DFC system									
12 ppbv NO	120	22.8	43.3	1.4	94.7	96.1	2.2	-73.4 (-72.2)	
12 ppbv NO	120	23.0	45.7	1.4	95.2	98.6	1.8	-72.8 (-71.6)	
12 ppbv NO	120	23.2	44.8	1.4	95.1	96.1	-6.1	-72.7 (-71.4)	
34 ppbv NO	120	24.1	27.8	4.2	105.1	93.6	-1.5	-69.5 (-68.4)	
34 ppbv NO	120	24.8	27.1	4.0	98.1	94.3	-0.2	-70.4 (-69.3)	
34 ppbv NO	120	25.1	26.8	4.1	102.4	91.1	-3.1	-70.1 (-69.0)	
34 ppbv NO	120	25.2	26.5	3.9	97.4	93.4	-0.1	-71.0 (-69.9)	
101 ppbv NO	120	23.0	33.8	12.0	99.5	94.7	6.0	-71.1 (-70.0)	18.9
101 ppbv NO	120	23.0	34.1	12.0	99.1	94.0	0.8	-69.3 (-68.2)	19.1
101 ppbv NO	120	23.3	34.4	11.9	98.7	92.0	-2.5	-71.6 (-70.5)	18.3
101 ppbv NO	120	23.4	34.6	11.5	95.7	95.3	-1.6	-72.0 (-70.9)	19.0
749 ppbv NO	120	22.6	45.6	14.0	97.8	93.6	3.6	-70.6 (-69.5)	21.2
749 ppbv NO	120	22.7	48.1	14.8	103.0	92.0	5.4	-70.7 (-69.6)	20.5
749 ppbv NO	120	22.9	48.3	13.6	94.7	88.0	-0.4	-70.2 (-69.1)	19.9

Sample	Time (min)	T (°C)	RH (%)	$NO_2^-+NO_3^-$ (μM)	Recovery (%)	NO_2^- percent (%)	P_{diff} (%)	$\delta^{15}N^a$ (‰)	$\Delta^{17}O$ (‰)
749 ppbv NO	120	23.0	48.2	14.6	101.7	89.3	5.6	-70.8 (-69.7)	20.9
NO collection – laboratory DFC system – temperature effect									
34 ppbv NO	120	12.0	90.9	4.1	102.6	90.2	7.6	-69.9 (-68.8)	
34 ppbv NO	120	11.4	92.0	4.0	100.3	90.9	0.9	-71.1 (-69.9)	
34 ppbv NO	120	11.2	92.4	4.0	100.2	86.1	0.7	-71.4 (-70.3)	
34 ppbv NO	120	11.3	92.7	3.9	96.1	89.8	0.3	-72.1 (-71.0)	
101 ppbv NO	120	30.6	28.7	12.6	104.5	85.3	-0.8	-71.7 (-70.6)	19.3
101 ppbv NO	120	30.7	28.3	11.3	94.2	92.4	7.2	-70.3 (-69.2)	20.0
101 ppbv NO	120	31.0	28.7	11.4	94.4	92.1	1.2	-72.1 (-70.9)	20.5
101 ppbv NO	120	31.0	29.4	11.8	98.1	88.2	6.5	-69.3 (-68.2)	20.2
NO collection – laboratory DFC system – interference									
34 ppbv NO + 500 ppbv NH_3	120	23.2	33.4	3.9	97.5	89.9	-3.7	-70.5 (-69.4)	
34 ppbv NO + 500 ppbv NH_3	120	23.0	33.0	4.0	98.4	88.3	-4.1	-68.6 (-67.5)	
34 ppbv NO + 500 ppbv NH_3	120	22.7	32.9	4.1	102.7	86.4	-3.7	-71.2 (-70.1)	
101 ppbv NO + 500 ppbv NH_3	120	23.2	47.4	11.3	94.1	96.8	-3.2	-71.0 (-69.9)	19.7
101 ppbv NO + 500 ppbv NH_3	120	23.1	46.7	11.8	98.1	89.8	3.2	-71.0 (-70.0)	18.0
101 ppbv NO + 500 ppbv NH_3	120	23.1	46.3	11.7	97.7	92.2	5.8	-71.4 (-70.3)	20.1
101 ppbv NO + 500 ppbv NH_3	120	23.0	45.7	12.0	100.3	87.1	4.4	-71.6 (-70.5)	20.0
101 ppbv NO + HONO scrubber	120	22.9	86.4	11.6	96.4	92.5	3.0	-71.1 (-70.0)	19.7
101 ppbv NO + HONO scrubber	120	22.1	90.0	11.5	95.6	89.0	10.1	-71.5 (-70.4)	19.8

Sample	Time (min)	T (°C)	RH (%)	$NO_2^-+NO_3^-$ (μM)	Recovery (%)	NO_2^- percent (%)	P_{diff} (%)	$\delta^{15}N^a$ (‰)	$\Delta^{17}O$ (‰)
101 ppbv NO + HONO scrubber	120	22.1	90.0	11.6	96.7	89.4	-9.7	-71.4 (-70.3)	20.0
101 ppbv NO + HONO scrubber	120	21.9	92.5	11.7	98.1	88.3	7.9	-70.2 (-69.1)	18.9
NO collection – field DFC system									
25 ppbv NO	120	21.7	39.2	3.3	108.3	94.3	15.9	-70.7 (-69.5)	
25 ppbv NO	120	21.4	40.7	3.2	104.9	98.8	6.3	-73.5 (-72.3)	
25 ppbv NO	120	21.3	41.3	3.0	100.1	91.5	-2.3	-74.0 (-72.9)	
25 ppbv NO	120	21.2	41.9	3.1	102.4	92.7	-2.6	-73.3 (-72.2)	
34 ppbv NO	120	22.5	48.5	3.7	91.3	99.7	-8.0	-71.1 (-70.0)	
34 ppbv NO	120	22.4	50.4	3.9	96.8	92.6	-2.7	-71.5 (-70.4)	
34 ppbv NO	120	21.5	51.0	4.1	102.7	88.1	3.2	-69.4 (-68.2)	
34 ppbv NO	120	21.3	51.8	4.0	99.6	90.8	0.2	-71.0 (-69.9)	
56 ppbv NO	120	21.7	43.9	6.1	95.1	95.4	-1.3	-72.4 (-71.4)	
56 ppbv NO	120	20.8	45.2	6.2	97.3	92.7	0.4	-71.1 (-70.1)	
56 ppbv NO	120	20.9	45.2	6.3	95.6	90.6	-4.9	-71.0 (-69.9)	
101 ppbv NO	120	22.2	35.3	11.4	93.9	90.9	6.9	-70.8 (-69.7)	19.8
101 ppbv NO	120	21.7	36.4	11.8	97.8	90.9	-9.8	-72.1 (-71.0)	
101 ppbv NO	120	21.5	37.1	12.0	98.9	87.5	1.7	-70.2 (-69.1)	19.6
101 ppbv NO	120	21.5	37.6	11.8	97.6	88.9	5.0	-70.8 (-69.8)	19.0
Mean					98.5	91.7	1.1	-71.1 (-70.0)	19.7
Standard error (1 σ)					3.5	3.4	5.1	1.1 (1.1)	0.8

a: Relative to N_2 in the air. $\delta^{15}N$ values before the isobaric correction are shown in the brackets.

Table S5. Complete dataset: NO collection, laboratory soil rewetting experiment.

Sample	Time (min)	T (°C)	RH (%)	$NO_2^-+NO_3^-$ (μM)	Recovery[a] (%)	NO_2^- percent (%)	Dilution factor	P_{diff} (%)	$\delta^{15}N$[b] (‰)	$\Delta^{17}O$ (‰)
Replicate 1										
1	30	23.6	62.7	9.2	105.1	95.4	1.7	3.3	-37.1 (-36.1)	19.4
2	30	23.3	60.6	7.6	100.9	95.6	1.4	-2.5	-38.8 (-37.7)	
3	30	23.1	60.0	5.6	110.0	89.6	1.0	1.1	-40.5 (-39.5)	
4	120	23.0	58.3	6.8	106.2	92.0	1.2	3.1	-49.3 (-48.3)	
5	120	23.0	56.7	5.5	104.4	89.2	1.0	-3.6	-52.9 (-51.9)	
6	120	22.6	45.6	7.4	93.3	97.6	1.3	6.0	-53.7 (-52.6)	
7	120	22.4	41.3	9.6	113.5	85.0	1.7	-0.4	-53.6 (-52.6)	18.8
Replicate 2										
1	30	24.4	61.1	9.3	102.6	96.4	1.7	5.4	-36.8 (-35.7)	18.8
2	30	23.3	62.4	9.0	106.2	94.5	1.6	4.7	-37.4 (-36.4)	17.7
3	30	23.0	62.6	6.4	109.4	88.9	1.2	4.6	-39.5 (-38.4)	
4	120	22.9	61.2	6.5	100.8	97.4	1.2	2.7	-47.8 (-46.7)	
5	120	22.9	46.7	8.5	96.5	95.4	1.5	1.7	-52.5 (-51.4)	
6	120	22.9	35.0	9.0	97.9	98.0	1.6	-2.1	-53.4 (-52.3)	19.4
7	120	23.0	28.4	5.5	93.5	88.6	1.0	4.0	-51.8 (-50.8)	
Replicate 3										
1	30	23.9	61.5	10.3	100.7	92.3	1.9	-5.5	-36.3 (-35.3)	18.4
2	30	23.2	60.4	8.7	97.7	93.2	1.6	4.0	-37.7 (-36.8)	
3	30	22.9	62.1	6.4	108.0	90.5	1.2	0.1	-39.6 (-38.6)	
4	120	22.8	59.1	6.2	98.4	93.5	1.1	9.9	-47.8 (-46.7)	
5	120	22.8	52.4	8.7	101.1	94.8	1.6		-50.6 (-49.5)	20.5
6			*not collected*							
7	120	22.7	38.7	6.1	97.6	91.6	1.1	-1.9	-52.8 (-51.8)	

Sample	Time (min)	T (°C)	RH (%)	$NO_2^-+NO_3^-$ (μM)	Recovery[a] (%)	NO_2^- percent (%)	Dilution factor	P_{diff} (%)	$\delta^{15}N$[b] (‰)	$\Delta^{17}O$ (‰)
Mean					102.2	92.9		1.8		19.0
Standard error (1 σ)					5.6	3.4		3.8		0.9

a: NO recovery was calculated by dividing the measured $NO_2^-+NO_3^-$ concentration by the theoretical concentration calculated using the collection time, sample flow rate (1.6 slpm), NO concentration measured in the chamber headspace, and the TEA solution volume. The TEA solution volume was corrected for evaporative loss by weighing the gas washing bottle containing the solution before and after each sample collection.

b: Relative to N_2 in the air. $\delta^{15}N$ values were corrected for the isobaric correction using the measured $\Delta^{17}O$ values. For those samples without sufficient mass for the $\Delta^{17}O$ measurement, an average $\Delta^{17}O$ value, 19.0‰, was used for the correction. $\delta^{15}N$ values before the isobaric correction are shown in the brackets.

Table S6. Complete dataset: NO collection, field rewetting experiment.

Sample	Time (min)	T (°C)	RH (%)	$NO_2^-+NO_3^-$ (μM)	Recovery[a] (%)	NO_2^- percent (%)	Dilution factor	P_{diff} (%)	$\delta^{15}N$[b] (‰)	$\Delta^{17}O$ (‰)
MilliQ addition										
1	120	22.1	71.3	15.9	105.7	86.3	2.8	8.8	-41.3 (-40.1)	20.7
2	120	28.2	70.1	23.1	101.5	91.3	1.3	5.8	-44.3 (-43.3)	18.7
3	120	27.8	72.6	22.5	96.4	90.0	1.3	6.8	-42.2 (-41.2)	18.8
NO_3^- addition										
1	120	26.1	70.4	10.8	112.6	88.8	1.9	8.3	-39.4 (-38.3)	19.7
2	120	28.4	68.8	21.1	104.6	93.4	1.2	9.0	-40.7 (-39.8)	18.0
3	120	28.3	70.7	23.6	102.1	91.7	1.3	6.6	-40.7 (-39.7)	18.7
NO_2^- addition										
1	45	20.6	74.8	7.0	96.4	95.6	1.2	3.7	-23.4 (-22.3)	
2	45	22.0	72.3	17.8	118.8	92.9	1.0	7.1	-25.6 (-26.6)	18.5
3	45	24.9	67.2	24.6	123.7	92.3	1.5	8.0	-28.2 (-27.2)	19.0
4	45	28.0	65.6	33.4	126.5	90.8	2.0	4.7	-30.9 (-30.0)	17.2
5	35	30.7	61.2	27.6	112.9	95.6	1.6	10.2	-32.3 (-31.4)	17.1
6	30	28.7	65.7	27.9	126.6	91.5	1.7	4.3	-34.4 (-33.4)	18.6
NH_4^+ addition										
1	120	20.7	67.0	5.7	96.4	88.2	1.0	7.2	-56.0 (-54.9)	
2	120	25.8	61.4	17.7	107.7	88.9	1.0	2.5	-59.8 (-58.7)	19.2
3	120	28.2	61.3	27.8	97.2	90.9	1.6	4.6	-57.6 (-56.6)	18.5
Mean					108.6	91.2		6.5		18.7
Standard error (1 σ)					11.0	2.6		2.2		0.9

a: NO recovery was calculated by dividing the measured $NO_2^-+NO_3^-$ concentration by the theoretical concentration calculated using the collection time, sample flow rate (1.6 slpm), NO concentration measured in the chamber headspace, and the TEA solution

volume. The TEA solution volume was corrected for evaporative loss by weighing the gas washing bottle containing the solution before and after each sample collection.

b: Relative to N_2 in the air. $\delta^{15}N$ values were corrected for the isobaric correction using the measured $\Delta^{17}O$ values. For those samples without sufficient mass for the $\Delta^{17}O$ measurement, an average $\Delta^{17}O$ value, 18.7‰, was used for the correction. $\delta^{15}N$ values before the isobaric correction are shown in the brackets.

REFERENCES

(1) Felix, J. D.; Elliott, E. M.; Shaw, S. L. Nitrogen isotopic composition of coal-fired power plant NO_x: influence of emission controls and implications for global emission inventories. *Environ. Sci. Technol.* **2012**, *46*(6), 3528-3535.

(2) Walters, W. W.; Goodwin, S. R.; Michalski, G. Nitrogen stable isotope composition ($\delta^{15}N$) of vehicle-emitted NO_x. *Environ. Sci. Technol.* **2015**, *49*(4), 2278-2285.

(3) Walters, W. W.; Tharp, B. D.; Fang, H.; Kozak, B. J.; Michalski, G. Nitrogen isotope composition of thermally produced NO_x from various fossil-fuel combustion sources. *Environ. Sci. Technol.* **2015**, *49*(19), 11363-11371.

(4) Fibiger, D. L.; Hastings, M. G.; Lew, A. F.; Peltier, R. E. Collection of NO and NO_2 for isotopic analysis of NO_x emissions. *Anal. Chem.* **2014**, *86*(24), 12115-12121.

(5) Fibiger, D. L.; Hastings, M. G. First measurements of the nitrogen isotopic composition of NO_x from biomass burning. *Environ. Sci. Technol.* **2016**, *50*(21), 11569-11574.

(6) Wojtal, P. K.; Miller, D. J.; O'Conner, M.; Clark, S. C.; Hastings, M. G. Automated, high-resolution mobile collection system for the nitrogen isotopic analysis of NO_x. *J. Vis. Exp.* **2016**, 118, e54962.

(7) Li, D.; Wang, X. Nitrogen isotopic signature of soil-released nitric oxide (NO) after fertilizer application. *Atmos. Environ.* **2008**, *42*(19), 4747-4754.

(8) Yang, W. X.; Meixner, F. X. Laboratory studies on the release of nitric oxide from sub-tropical grassland soils: The effect of soil temperature and moisture. In *Gaseous Nitrogen emissions from grasslands*; Jarvis, S. C.; Pain, B. F. Eds.; Cab International: 1997; pp 67-71.

(9) Van Dijk, S. M.; Gut, A.; Kirkman, G. A.; Gomes, B. M.; Meixner, F. X.; Andreae, M. O. Biogenic NO emissions from forest and pasture soils: Relating laboratory studies to field measurements. *J. Geophys. Res. Atmos.* **2002**, *107*(D20).

(10) Pape, L.; Ammann, C.; Nyfeler-Brunner, A.; Spirig, C.; Hens, K.; Meixner, F. X. An automated dynamic chamber system for surface exchange measurement of non-reactive and reactive trace gases of grassland ecosystems. *Biogeosciences*, **2009**, *6*(3), 405-429.

(11) Yu, Z.; Slater, L. D.; Schäfer, K. V.; Reeve, A. S.; Varner, R. K. Dynamics of methane ebullition from a peat monolith revealed from a dynamic flux chamber system. *J. Geophys. Res. Biogeosci.* **2014**, *119*(9), 1789-1806.

(12) Davidson, E. A.; Savage, K. V. L. V.; Verchot, L. V.; Navarro, R. Minimizing artifacts and biases in chamber-based measurements of soil respiration. *Agr. Forest Meteorol.* **2002**, *113*(1), 21-37.

(13) Xu, L.; Furtaw, M. D.; Madsen, R. A.; Garcia, R. L.; Anderson, D. J.; McDermitt, D. K. On maintaining pressure equilibrium between a soil CO2 flux chamber and the ambient air. *J. Geophys. Res. Atmos.* **2006**, *111*(D8).

(14) Jones, M. N. Nitrate reduction by shaking with cadmium: alternative to cadmium columns. *Water Res.* **1984**, *18*(5), 643-646.

(15) Sigman, D. M.; Casciotti, K. L.; Andreani, M.; Barford, C.; Galanter, M. B. J. K.; Böhlke, J. K. A bacterial method for the nitrogen isotopic analysis of nitrate in seawater and freshwater. *Anal. Chem.* **2001**, *73*(17), 4145-4153.

(16) Casciotti, K. L.; Sigman, D. M.; Hastings, M. G.; Böhlke, J. K.; Hilkert, A. Measurement of the oxygen isotopic composition of nitrate in seawater and freshwater using the denitrifier method. *Anal. Chem.* **2002**, *74*(19), 4905-4912.

(17) Coplen, T. B.; Böhlke, J. K.; Casciotti, K. L. Using dual- bacterial denitrification to improve $\delta^{15}N$ determinations of nitrates containing mass- independent ^{17}O. *Rapid Commun. Mass Spectrom.* **2004**, *18*(3), 245-250.

(18) Fuchs, H.; Dubé, W. P.; Lerner, B. M.; Wagner, N. L.; Williams, E. J.; Brown, S. S. A sensitive and versatile detector for atmospheric NO_2 and NO_x based on blue diode laser cavity ring-down spectroscopy. *Environ. Sci. Technol.* **2009**, *43*(20), 7831-7836.

(19) Atkinson, R.; Arey, J. Gas-phase tropospheric chemistry of biogenic volatile organic compounds: a review. *Atmos. Environ.* **2003**, *37*, 197-219.

(20) *Chemical Kinetics and Photochemical Data for Use in Atmospheric Studies Evaluation Number 15*; Jet Propulsion Laboratory, National Aeronautics and Space Administration: Pasadena, CA, 2006; https://trs.jpl.nasa.gov/handle/2014/41648.

(21) Dubé, W. P.; Brown, S. S.; Osthoff, H. D.; Nunley, M. R.; Ciciora, S. J.; Paris, M. W.; McLaughlin, R. J.; Ravishankara, A. R. Aircraft instrument for simultaneous, in situ measurement of NO_3 and N_2O_5 via pulsed cavity ring-down spectroscopy. *Rev. Sci. Instrum.* **2006**, *77*(3), 034101.

(22) Atkinson, R.; Baulch, D. L.; Cox, R. A.; Crowley, J. N.; Hampson, R. F.; Hynes, R. G.; Jenkin, M. E.; Rossi, M. J.; Troe, J.; Subcommittee, I. U. P. A. C. Evaluated kinetic and photochemical data for atmospheric chemistry: Volume II–gas phase reactions of organic species. *Atmos. Chem. Phys.* **2006**, *6*(11), 3625-4055.

(23) Michalski, G. and Bhattacharya, S.K. The role of symmetry in the mass independent isotope effect in ozone. *PNAS* **2009**, *106*(14), 5493-5496.

(24) Liu, Q.; Schurter, L. M.; Muller, C. E.; Aloisio, S.; Francisco, J. S.; Margerum, D. W. Kinetics and mechanisms of aqueous ozone reactions with bromide, sulfite, hydrogen sulfite, iodide, and nitrite ions. *Inorg. Chem.* **2001**, *40*(17), 4436-4442.

(25) Savarino, J.; Bhattacharya, S. K.; Morin, S.; Baroni, M.; Doussin, J. F. The NO+O_3 reaction: A triple oxygen isotope perspective on the reaction dynamics and atmospheric implications for the transfer of the ozone isotope anomaly. *J. Chem. Phys.* **2008**, *128*(19), 194303.